NTNU
Norwegian University of Science and Technology

Characterization of new mouse model lacking DNA repair factor MRI

Growth and neural development in mice deficient
of DNA repair factor MRI

Øystein Røsand

Molecular Medicine (2 year)

Submission date: June 2019

Supervisor: Valentyn Oksenych, Department of Clinical and Molecular Medicine (NTNU)

Norwegian University of Science and Technology

Department of Clinical and Molecular Medicine

Acknowledgement

This project was written as part of a MSc in Molecular Medicine at the Department of Clinical and Molecular Medicine (Faculty of Medicine and Health Science, NTNU, Trondheim). The master thesis was conducted in the Non-Homologous End-Joining group headed by Valentyn Oksenych, PhD.

First of all, I want to thank my supervisor, Valentyn Oksenych, for all the advice and encouragement you have provided. I appreciate the help, close follow-up and knowledge you have bestowed me. You have been willing to challenge and support me during the past year, which has helped me succeed. For all this, and more, I am truly thankful.

Wei Wang, thank you for all help regarding neurosphere experiments, and for being patient while I learned. I appreciate your willing to teach me the techniques required for me to succeed. A huge tank you to Ping Ji for always reaching out a helping hand.

To all members of our group and others working in the lab – thank you for all the help and support during the last year, and for showing me your ways. It has been a pleasure working with you. A special thanks to Mengtan Xing and Sergio Castaneda for everything you have taught me in the lab.

Last but not least – I want to thank my friends and family for all support and encouragement, it has meant a lot to me.

Abstract

Double-strand breaks (DSBs) are constantly generated in the DNA by endogenous and exogenous agents. In mammalian cells, DSBs activate DNA damage responses (DDRs) to repair the lesions. One major DSB repair pathway is non-homologous end-joining (NHEJ), which is active throughout the cell cycle and is especially required for the homeostasis of post-mitotic neurons in the brain. NHEJ involves a variety of factors; some are essential and evolutionary conserved, while other are accessory and only required for specific types of lesions. To determine the roles of specific NHEJ factors, genetic inactivation of the corresponding NHEJ genes has been established in mice. Previously, several mouse models lacking one or multiple proteins has been generated and characterized. For this project, a mouse model lacking an accessory NHEJ factor named modulator of retroviral infection (MRI) was developed and characterised. The first aim of this project was to investigate the impact of MRI deficiency on growth and neural development in our *Mri* mouse model. This was done by comparing the body weight and size of $Mri^{-/-}$ and WT mice. To determine the effect of *Mri* inactivation on neural development, brains from WT and $Mri^{-/-}$ mice were isolated, and neurosphere cultures were established. These cultures were used to compare WT and $Mri^{-/-}$ neural stem progenitor cell (NSPC) proliferation, self-renewal and differentiation. The *Mri* knockout model was here found to be indistinguishable from WT mice in relation to growth, NSPC self-renewal and differentiation. However, $Mri^{-/-}$ NSPC have impaired proliferation. This suggest that MRI support cellular proliferation during mammalian neurogenesis. The second aim of this project was to investigate genetic interaction between MRI, XLF, PAXX, DNA-PKcs and p53. For this aim, 89 pups were analysed, however, further studies are required to make a solid conclusion.

Table of Contents

List of Figures

List of Tables

Abbreviations

Ag	Antigen
ATM	Ataxia telangiectasia mutated
ATR	Ataxia telangiectasia and Rad3-related
BCR	B cell receptor
bp	Base pair
BSA	Bovine serum albumin
CD	Cluster of differentiation
CSR	Class switch recombination
CYREN	Cell cycle regulator of NHEJ
D	Diversity
DDR	DNA damage response
DMEM	Dulbecco's modified eagle medium
DN	Double negative
DNA-PKcs	DNA-dependent protein kinase catalytic subunit
DSB	Double strand break
FBS	Fetal bovine serum
G_0	Resting phase in the cell cycle
G_1	First gap phase in the cell cycle
G_2	Second gap phase in the cell cycle
H-chain	Heavy chain
HR	Homologous recombination
HSC	Hematopoietic stem cell
Ig	Immunoglobulin
IR	Ionizing radiation
J	Joining
Ku	Ku70/Ku80 heterodimer
L-chain	Light chain
Lig4	DNA ligase IV
M	Mitosis phase

Min	Minute
MRI	Modulator of retroviral infection
NHEJ	Non-homologous end-joining
PAXX	Paralogue of XRCC4 and XLF
PBS	Phosphate-buffered saline
PCR	Polymerase chain reaction
RAG1/2	Recombination activation gene 1 and 2
RPM	Revolutions per minute
RSS	Recombination signal sequence
S	Synthesis phase
SCID	Severe combined immunodeficiency
SHM	Somatic hypermutation
SP	Single positive
SSB	Single strand break
TBE	Tris-borate-EDTA
T_C	T cytotoxic cell
TCR	T cell receptor
T_H	T helper cell
Trp53	Transformation related protein 53, gene encoding p53
V	Variable
V(D)J	Variable(diversity)joining
WT	Wild type
XLF	XRCC4-like factor
XRCC4	X-ray repair cross-complimenting protein 4

1 Introduction

1.1 Lymphocyte development

The production of new lymphocytes is called lymphopoiesis and takes place in specialised lymphoid tissues, such as the bone marrow and the thymus, which are part of the central lymphoid tissues. All cells of the immune system are derived from hematopoietic stem cells (HSCs) in bone marrow. HSCs differentiate through a series of progenitor stages, eventually giving rise to mature lymphocytes. Lymphocytes are derivatives of white blood cells, which include T and B cells. During lymphopoiesis, progenitor T cells migrate from the bone marrow to the thymus where they complete their maturation into naïve T cells. However, most HSCs remaining in the bone marrow mature into B cells [1]. Finally, T and B cells migrate and complete their maturation in the peripheral lymphoid tissues, such as the spleen, lymph nodes and mucosal lymphoid tissue. One of the major goals of lymphopoiesis is to enable the host to perform adaptive immune responses against the wide range of pathogens by generating diverse T and B cell receptors on the respectively circulating T and B cells. It is therefore important that those lymphocytes that mature carry useful antigen receptors with the ability to recognise pathogens and not react against the host itself. Rigorous testing is therefore used to positively select for non-self-interacting lymphocytes, and to negatively select for those who are strongly self-reactive. Lymphocytes that are negatively selected are terminated through death by apoptosis. In fact, a majority of developing lymphocytes die before leaving the central lymphoid organs [2].

1.1.1 B cells

B cells and antibodies that they produce play a central role in the adaptive immune system. The origin of B cells can be traced back to the evolution of adaptive immunity more than 500 million years ago [3]. As earlier explained, B cells develop from HSCs that originate from the bone marrow. The bone marrow functions as a specialised microenvironment, providing signals that promote activation of genes, which direct the development from HSCs to lymphocyte progenitors and the consecutive differentiation into B cells. In the bone marrow, B cells pass through several developmental stages, during which they acquire their antigen specificity [4]. The HSCs differentiate first into multipotent progenitor cells (MPPs). MPPs have the ability to produce myeloid and lymphoid cells. MPPs mature into pro-B cells with the induction of the B-lineage-specific transcription factor E2A [5, 6]. The remaining stages of B cell development are, in chronological order, early pro-B cell, late pro-B cell, small pre-B cell, immature B cell, and mature B cell [2]. A major goal of B cell development is to produce a wide range of diverse and functional B cell receptors (BCRs). The BCR is composed of two heavy-chains (H-chains) and two light-chains (L-chains), κ or λ. BCR development involves rearrangement of the H-chain V_H, D_H and J_H variable gene segments, as well as rearrangement of κ or λ L-chain V_L and J_L variable gene segments. Rearrangement of the H-chain occur first which, if found successful, initiate pre-B cell proliferation and subsequent L-chain rearrangement. Successive L-chain rearrangement results in complete immunoglobulin BCR formation. The V_H, D_H and J_H segments of the BCR combined with V_L and J_L of the BCR are referred to as the variable region of the BCR, where antigen-recognition takes place [5]. Schematic overview of the BCR is illustrated in Figure 1.1.

Figure 1.1: The BCR, composed of two H-chains and two L-chains, consisting of variable and constant regions. The constant regions are indicated in blue. The H-chain variable region have V (green), D (red) and J (orange) segments. The L-chain variable region only consists of a V and a J segment.

As previously mentioned in Section 1.1.1, to prevent un-responsive and self-reactive lymphocyte formation and proliferation, developing B cells undergo positive and negative selection processes [7]. When the BCR is fully formed, the pre-B cell becomes an immature B cell. These cells are also called IgM due to a constant H-chain region named mu (μ-chain). Reaching the immature stage, B cells migrate from the bone marrow to secondary lymphoid organs. Differentiation in secondary lymphoid organs are mediated by dynamic changes in the expression pattern of many genes. Once the B cell encounter antigens (Ag), development continues and immature-B cells become mature-B cells. Mature B lymphocytes adjust immunoglobulin specificity via somatic hypermutation (SHM) and class switch recombination (CSR). The goal of SHM and CSR is to alter antibody function and affinity, which is crucial for the tailored specificity of the adaptive immune system. SHM introduces single point mutations in the H- and L-chain variable regions, resulting in altered BCR specificity and affinity. CSR involves a replacement of the constant μ-chain regions, resulting in an isotype switch from IgM to IgG, IgA or IgE. Furthermore, isotype switching changes the effector function of the antibody (Ab). Depending on the Ag activation, mature-B cells will either become plasma cells which produce large amounts of antibodies, or memory cells which will be activated at a later time point [2, 4, 8].

1.1.2 T cells

Like B cells, T cells derive from multipotent HSC in the bone marrow, and experience similar rearrangement of antigen-receptor genes and sequential testing. However, in contrast to B cells, progenitor-T cells migrate from the bone marrow to the thymus where they develop and mature. In the thymus, progenitor-T cells receive signals from the thymic epithelial cells to further commit to the T cell lineage. This commitment induces the expression of genes important for T cell receptor (TCR) assembly [2]. The TCR can either be composed of α and β receptor chains (TCRαβ), or γ and δ receptor chains (TCRγδ). Similar to the BCRs, the TCRs contain constant regions and variable *V*, *D* and *J* regions, which need to be rearranged to produce functional TCRs. *V* and *J* segments are present at all TCR loci, whereas only β and δ TCR loci contain *D* segments [9, 10]. Example of the TCRαβ is presented in Figure 1.2.
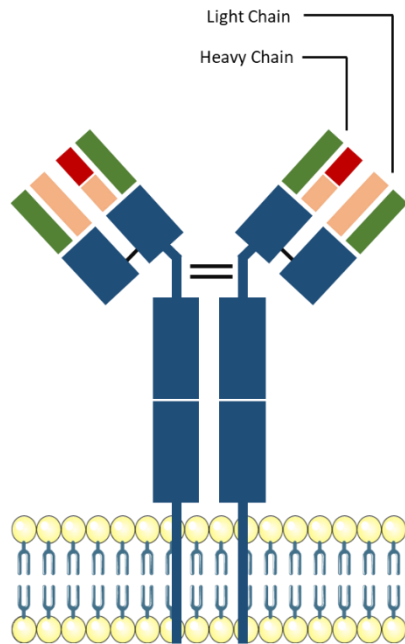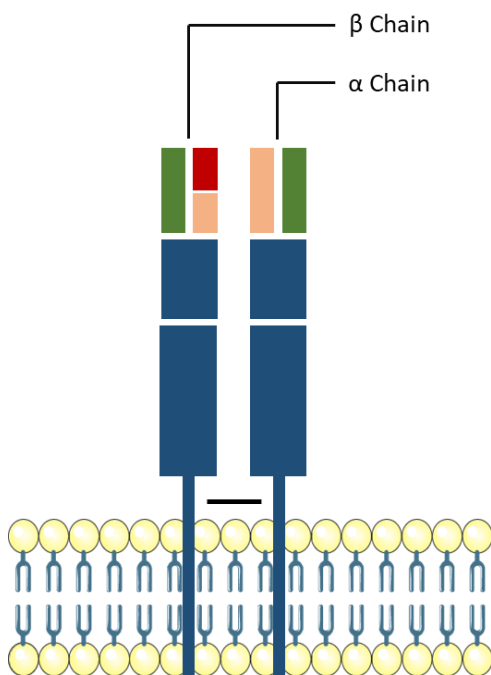

Figure 1.2: The TCRαβ, composed of a β and α chain, consisting of variable and constant regions. Constant regions are indicated in blue. The β chain have V (green), D (red) and J (orange) segments. The α chain variable region consists of a V and a J segment.

The developmental stages of T cells are characterised by the expression of TCR, co-receptor proteins, e.g. CD4 and CD8, and expression of cell surface proteins, e.g. CD3. During early development, T cells are divided into distinct developmental stages based on the lack of CD4 and CD8 expression (double negative). These stages are arranged as followed; DN1, DN2, DN3 and DN4 [10]. Rearrangement of the β/δ receptor chain variable region occurs during the DN2 stage. Then, during the DN3 stage, rearranged β/δ receptor chain assembles with CD3 and a surrogate α/γ chain creating a pre-TCR. Finally, during DN4, the α/γ receptor chain rearranges and replace the surrogate chains, creating the TCRαβ or TCRγδ [2]. Surface expression of TCRαβ or TCRγδ marks the transition from a pre-TCR to a double-positive (DP)-TCR (CD4$^+$CD8$^+$). Finally, antigen involved positive and negative selection processes drive further differentiation resulting in CD4$^+$ or CD8$^+$ T cells [4]. CD4$^+$ T cells commit to the T helper lineage (T$_H$), which activates other cells of the immune system, such as B cells [11]. Moreover, CD8$^+$ T cells are committed to the T cytotoxic lineage (T$_C$), which mediates lysis of infected target cells [12]. Example of T cell development is presented in Figure 1.3.
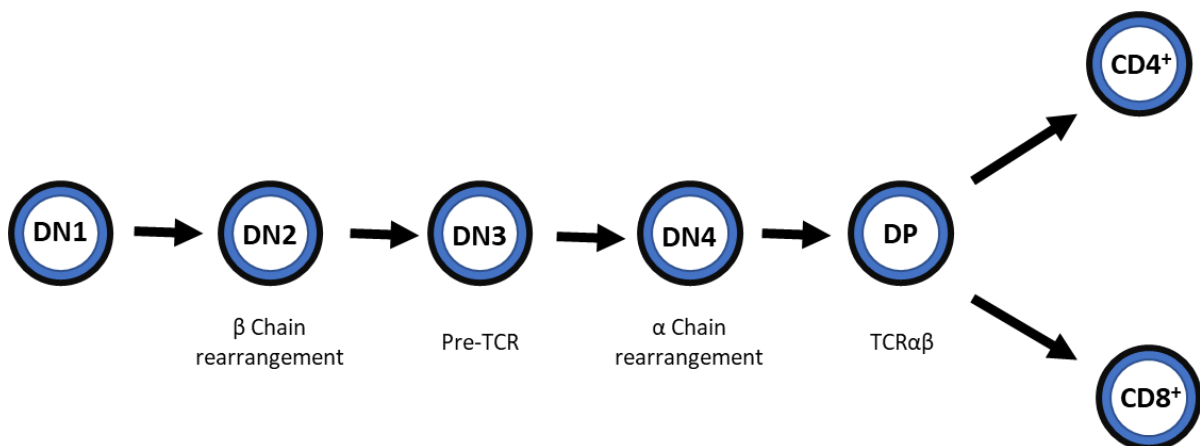
Figure 1.3: Development of T cells from DN1 cells to CD4$^+$ or CD8$^+$ T cells in the thymus.

1.1.3 V(D)J recombination

As mentioned in earlier sections, BCRs and TCRs have variable *V*, *D* and *J* gene segments that are rearranged to increase the receptor specificity and sensitivity. The process responsible for this rearrangement is called V(D)J recombination [2]. This is a site-specific recombination process that only functions during the development of lymphocytes. V(D)J recombination occurs between two gene segments which are flanked by conserved recombination signal sequences (RSSs). RSSs consist of conserved heptamer and nonamer sequences, separated by 12 and 23 nucleotides of less conserved spacer sequences [13]. V(D)J recombination is mechanistically divided into two phases; cleavage and repair. The cleavage is initiated by the recombination activating genes 1 and 2 (RAG1 and RAG2, RAG1/2), which are two lymphocyte specific endonucleases. RAG1/2 can recognise the RSSs and introduce a single strand nick between the *V*, *D* and *J* segments and the RSSs. Then, through transesterification, two hairpin coding ends and two blunt signal ends are formed [14]. Before the coding and signalling ends are processed and ligated, RAG1/2 retain them as a post-cleavage complex (PCC). Before ligation, hairpin coding ends need to be opened by additional processing. Opened coding ends are joined into coding joints by the NHEJ machinery. Signal ends does not require further processing before being joined [15, 16]. An overview of V(D)J recombination is presented in Figure 1.4.
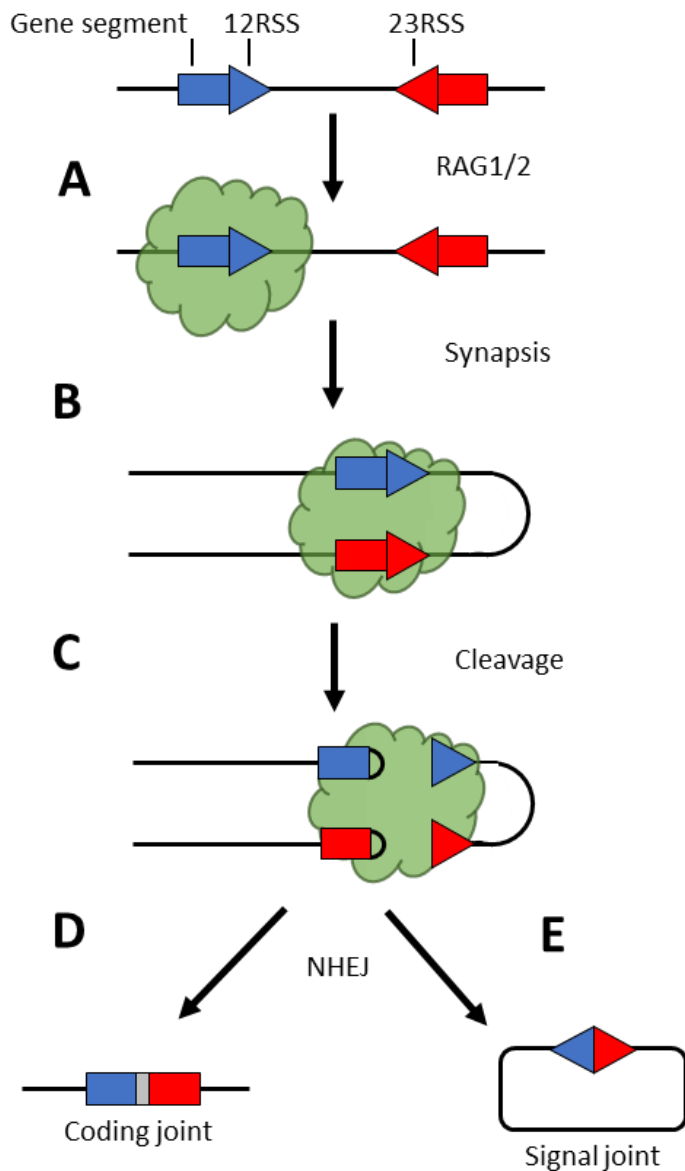
Figure 1.4: A simplified illustration of V(D)J recombination. **A**) Antigen receptor gene segments flanked by a 12RSS or a 23RSS are recognized and bound by RAG1/2. **B**) Synapsis and nicking of RSSs adjacent to segments being joined by RAG proteins. **C**) Double strand cleavage and hairpin formation of coding ends. **D**) Hairpin opening by Artemis, end-processing, and end-joining by NHEJ factors. Processing of ends often results in nucleotide loss and addition (represented in grey). **E**) NHEJ of signal ends, forming the signal joint.

1.2 DNA repair

Our genome is constantly under attack by genotoxic agents, which are threatening our genomic integrity. It has long been estimated that the mammalian genome experiences $\sim 10^5$ DNA lesions each day [17]. DNA damage can be caused by exogenous agents, e.g. ionizing radiation (IR) or ultraviolet (UV) light, and endogenous agents, e.g. mitochondrial respiration or replication stress. Assault by DNA damaging factors may cause DNA lesions and breaks. Persistent damage can induce mutagenesis, such as insertions/deletions or single base substitutions, in addition to gross chromosomal rearrangements, e.g. chromosomal translocations or inversions. Moreover, DNA damage can result in various forms of single- and double-strand breaks (SSB and DSB respectively). Failure to repair DNA damages can have severe consequences, including immunodeficiency, neurodegeneration and susceptibility to cancer development. Cells have therefore adapted several DNA repair pathways to ensure preservation of the genome stability [18, 19].

1.2.1 DNA Double-Strand Breaks

One of the most deleterious form of DNA damage is double strand breaks. In some cases, a single DSB is sufficient to disturb a cells genomic integrity, or even kill it. Mammalian cells have therefore evolved highly efficient DSB repair pathways [20]. In some cases, DNA DSB are required as part of natural physiological processes, such as previously explained V(D)J recombination and CSR. There are two major DSB repair pathways; the homologous recombination (HR) pathway and the non-homologous end-joining (NHEJ) pathway [19, 21]. The HR pathway requires an intact homologous template and is thus only active during the S^A- and $G_2{}^B$ phase. Because HR utilises homologous template strand, DSBs repair is error free [22]. In contrast to HR, NHEJ does not require a template strand and can therefore function throughout the entire cell cycle. NHEJ is thus the most prominent pathway of for DNA DSB repair in mammalian cells, especially in $G_0{}^C$ and $G_1{}^D$ phase where template strands are absent [18].

[A] S: Synthesis phase, DNA replication. Occurs between the G_1 and G_2 phase
[B] G_2: Second gap phase, cell growth. Cells in this phase are preparing for mitosis
[C] G_0: Resting state, non-dividing cells
[D] G_1: First gap phase, cell growth

1.2.2 Non-Homologous End-Joining

NHEJ is a key DNA repair factor in higher eukaryotes. The pathway involves recognition and ligation of the DSBs by four core factors; Ku70 and Ku80, DNA Ligase IV (Lig4), and X-ray Repair Cross-Complementing protein 4 (XRCC4). These core factors are essential and evolutionary conserved [23]. In addition, there are several accessory factors which contribute at different stages of the NHEJ pathway. These factors are; DNA-dependent protein kinase catalytic subunit (DNA-PKcs), Artemis, XRCC4-like factor (XLF), Paralogue of XRCC4 and XLF (PAXX) and modulator of retroviral infection (MRI) [24]. The NHEJ can be divided into three major steps: i) detection of the DSB, ii) DNA end processing for ligation preparation, iii) ligation of two suitable DNA ends [18]. To initiate NHEJ, Ku70 and Ku80 bind at both ends of the DSBs, forming a ring-shaped heterodimer (Ku). The presence of Ku on the DSB inhibits other DNA repair pathways and is therefore considered the NHEJ fate-determining step [19]. Direct ligation of the DSBs is often impeded due to chemical modifications or mismatching overhangs. Therefore, processing of the ends is required before ligation can occur. The Ku-DNA complex recruits DNA-PKcs, which help stabilise and align the DNA ends. DNA-PKcs is further activated through autophosphorylation, resulting in the activation of downstream factors, e.g. nucleases, kinases, polymerases and phosphatases. Artemis, an endonuclease, is one of the most prominent factors activated by DNA-PKcs, and facilitate DNA end processing [19, 25]. Furthermore, Ku also recruit PAXX, which helps to promote and stabilise the remaining NHEJ factors [26, 27]. Once appropriate DNA termini has been achieved, Ku recruits XLF and the XRCC4-Lig4 complex. XRCC4 interacts with Lig4 and XLF to form filamentous structures that bind and organize the DNA near the DSB, therefore playing a central scaffolding role in the NHEJ pathway [28]. Finally, XLF interact with XRCC4 and Lig4 to stimulate ligation of the broken ends. NHEJ is therefore an error prone process and, in addition to direct end joining, may result in insertions, deletions and translocations [18]. An overview of the NHEJ pathway and its factors is presented in Figure 1.5.
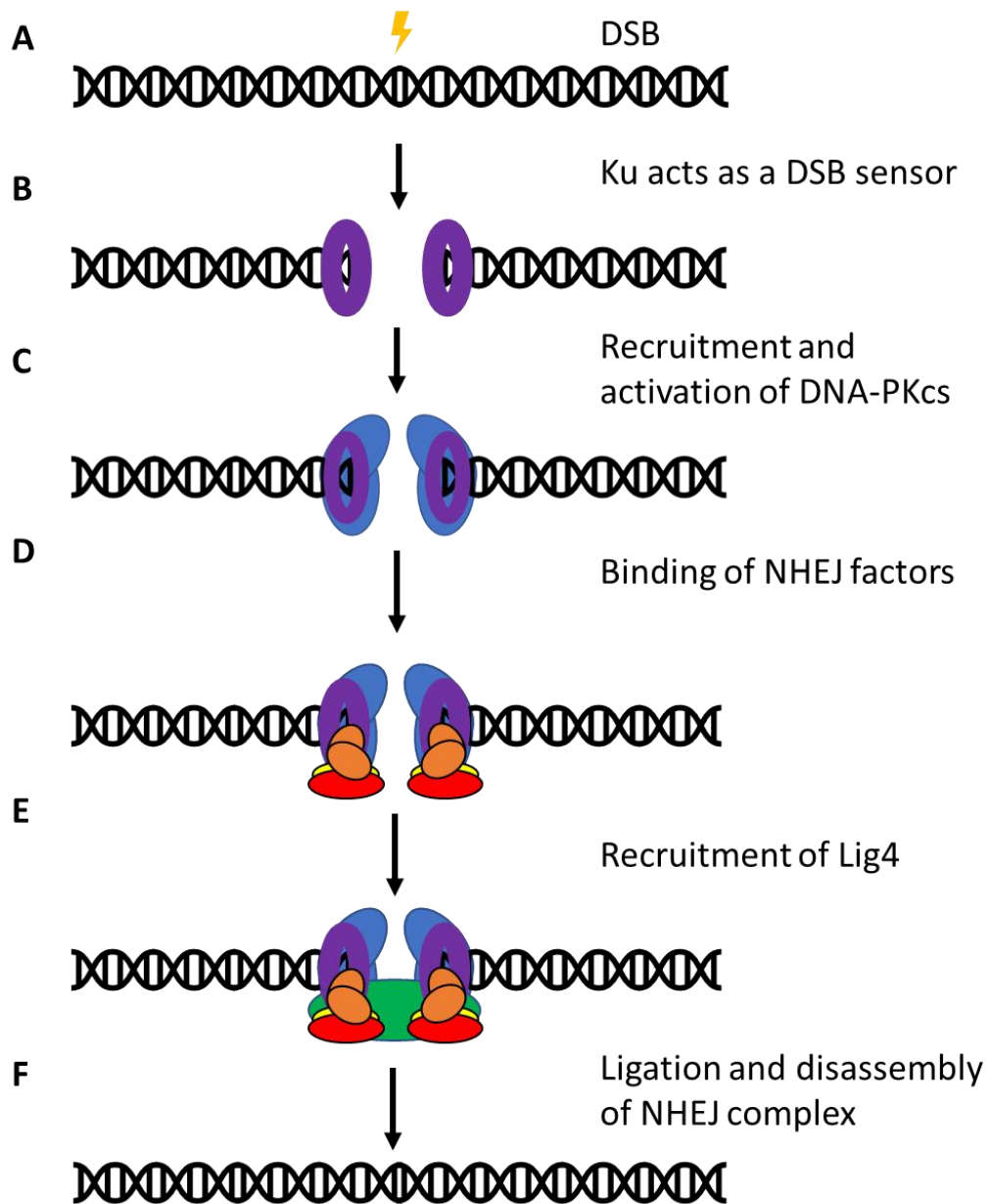
Figure 1.5: Simplified overview of the NHEJ pathway. **A**) DSB generated by endogenous and exogenous agents. **B**) Ku (purple) recognize and bind both ends of the break. **C**) DNA-PKcs (blue) is recruited and activated at the site of DSB. **D**) Binding of accessory NHEJ factors (orange, red and yellow). **E**) End processing to create ideal termini, and the recruitment of XRCC4/Lig4 complex (green). **F**) Ligation and complex disassembly.

1.2.4 Modulator of retroviral infection / Cell cycle regulator of NHEJ

The modulator of retroviral infection, known as MRI, is a recently discovered NHEJ factor. MRI was first reported by Agarwal, S. *et al.* (2006) [29]. In humans, the MRI coding gene (*Mri*) is located on chromosome 7 and was initially named "open reading frame 49" (C7orf49). As the name suggests, it was initially found to have the ability to reverse the resistance to retroviral infection in a mutant cell line [29]. Later work showed that MRI co-localizes to the nucleus with the Ku complex, with an increased concentration of MRI upon induction of DNA DSB, resulting in an enhanced rate of NHEJ *in vitro* [30]. This is further supported by the discovery that MRI possesses an N-terminal Ku-binding motif (KBM), which is conserved among vertebrates. In addition, studies have revealed a distinct but related C-terminal motif present in XLF, PAXX and MRI, named the XLF-like motif (XLM) [31]. MRI is therefore considered to be a novel NHEJ factor. However, MRI has been suggested to inhibit NHEJ at the S and G_2 phases of the cell cycle. This suggestion was based on results showing that by binding to Ku, MRI inhibit NHEJ-mediated chromatid fusion upon telomer deprotection. MRI has therefore been given an addition name: the cell cycle regulator of NHEJ (CYREN) [32].

Previous published *Mri* knock out mouse models (2018) show an increased sensitivity to IR when compared to WT. However, $Mri^{-/-}$ cells showed a lower level of sensitivity to IR than other cells with deficient for NHEJ factors, such as XLF. Furthermore, murine $Mri^{-/-}$ B cells have been proven to exhibit modest defects in Ig CSR. Moreover, $Mri^{-/-}Xlf^{-/-}$ mice have been shown to exhibit embryonic lethality, indicating functional redundancy between MRI and XLF in mice, as both single knock out *Mri* and *Xlf* mice are viable without any overt phenotype [33]. Similar phenotypes have been shown in mice deficient for core NHEJ factors such as Lig4 and XRCC4, in addition to combine deficiencies of XLF and PAXX, and XLF and DNA-PKcs [24, 34, 35]. No human patients with mutations in *MRI* gene have been reported. However, it has been demonstrated that MRI is indeed important during the repair of IR- and chemically induced DNA DSBs in murine cells [30, 33].

1.2.5 Interaction between NHEJ and p53

Preservation of genome integrity is crucial for preventing disease, e.g. cancer. The tumour suppressor p53, also known as the guardian of the genome, is one of the key proteins in highly conserved tumour suppressing mechanisms. p53 prevents uncontrolled proliferation of DNA damaged cells by either mediating cell cycle arrest, or initiating cell death through apoptosis. Upon DSBs, ataxia telangiectasia mutated (ATM) and ataxia telangiectasia and Rad3-related (ATR) protein kinases phosphorylate and regulate the activity of several downstream factors which are involved in DNA repair, e.g. p53 and H2AX [36]. This cascade culminates in the G1/S checkpoint where p53 induces expression of p21 resulting in cell cycle arrest. Since repair of some DSBs by NHEJ can take a long time, this arrest provides an important opportunity for the cell to restore the genome before replication. Cells able to restore the integrity of DNA is allowed to proceed further down the cell cycle, while the cells with persistent damage undergo apoptosis mediated through p53 signalling. Overall, p53 functions as a crucial link between upstream signalling and activation of downstream signalling cascades [37].

Earlier studies with mice deficient in the NHEJ factors XRCC4 and Lig4, and double deficient in XLF/PAXX or XLF/DNA-PKcs are embryonically lethal [24, 34, 35, 38]. The inactivation of p53 has been shown to rescue the lethality of these NHEJ deficiencies [35, 39-41], highlighting the interactions between p53 and NHEJ during growth and development.

1.3 NHEJ deficiencies in patients

NHEJ deficiency causes increased radiation sensitivity and results in severe combined immune deficiency (SCID). The phenotypic severity is dependent on the inactivated NHEJ gene and type of mutation. SCID is defined as a group of disorders that affect both humoral and cellular immunity [42]. Human patients with mutations in *LIG4* [43, 44], *XRCC4* [45], *ARTEMIS* [46], *XLF* [42, 47], and *DNA-PKcs* (*PRKDC*) [48, 49] have been identified. However, patients with mutations in *KU70*, *KU80*, *PAXX* and *MRI* have yet not been reported. In addition to increased radiosensitivity and SCID, patients with mutated NHEJ genes may also be subject to growth defect, microcephaly, developmental delay, and cancer susceptibility. The different phenotypes observed in patients highlight the importance of NHEJ for the immune system, growth and development in humans.

1.4 Neural stem cells and neurogenesis

Neurogenesis is a process where cells of the nervous system are produced by neural stem progenitor cells (NSPCs). These cells include, but are not exclusive to, astrocytes and neurons. In the mammalian brain, neural stem cells can be found in two distinct regions: the sub-granular zone (SGZ) of the hippocampus [50], and the sub-ventricular zone (SVZ) in the lateral walls of the lateral ventricles [51]. These regions are also referred to as stem cell niches as they are specific microenvironments that maintain NSPC multipotency [52]. Under normal physiological conditions, NSPC aid in the maintenance of brain homeostasis [53]. However, during pathophysiological conditions, NSPC have been proposed to be involved in neuronal replacement [54]. Neurogenesis can be divided up in several stages, i) proliferation of NSPC, ii) production of multipotent daughter cells (self-renewal), iii) differentiation into specialised cells of the nervous system. The balance between these stages ensure appropriate neurogenesis.

Cell proliferation is achieved through cell growth and division, and can be defined as an increase in total cell number. In tissues, proliferation is influenced by division frequency, fraction of non-proliferative and proliferative daughter cells, and size of initial progenitor pool. Regulation of cell proliferation in the central nervous system (CNS) is very important, as circuit formation is dependent on the number of neurons produced during development. Moreover, the final number of neurons in the CNS are determined by NSPC proliferation initiation and termination. This can be regulated by many mechanisms, e.g. growth factors stimulation or hormone signal initiated metabolic changes. Defects in NSPC proliferation can cause neurodevelopmental disorders, such as Megalencephaly and Microcephaly [55].

Self-renewal is the process by which stem cells divide symmetrically or asymmetrically to generate one or two multipotent daughter cells, which subsequently divide symmetrically and finally differentiate [56]. Symmetric division is predominantly used when in need of cell expansion, e.g. during development or after injury. Whereas, asymmetric division is used to maintain the balance between stem cells and differentiated cells. For NSPC, self-renewal is division with maintenance of multipotency. The ability to self-renew is crucial for the expansion of stem cells, and the restauration of cell numbers after injury. Although similar, self-renewal and proliferation are not the same. While proliferation is a term that incorporates both stem and progenitor cells, self-renewal requires that at least one of the daughter cells

maintain their multipotency [57]. An overview of symmetric and asymmetric cell division is illustrated in Figure 1.6.
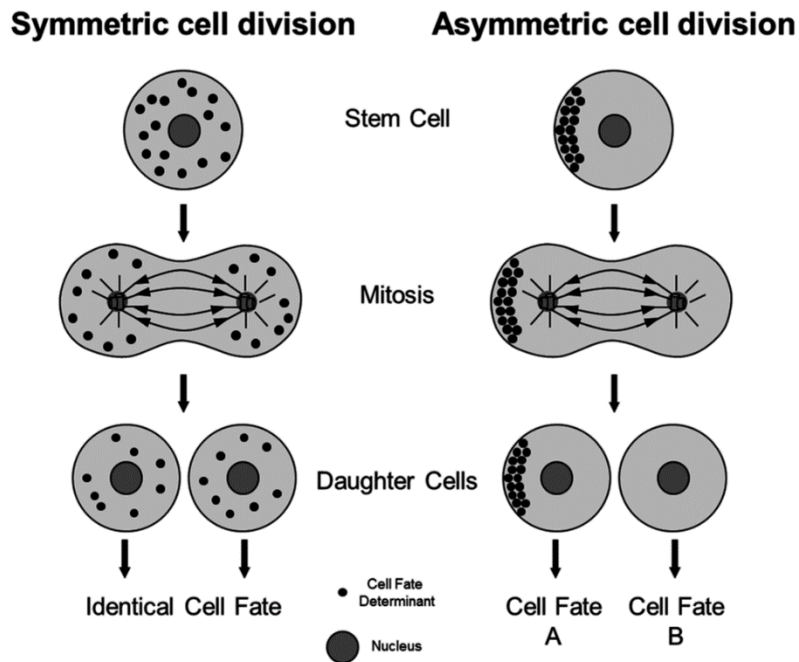
Figure 1.6: Overview of symmetric and asymmetric cell division, utilised for rapid cell expansion and cell development, respectively [58].

Differentiation is the process where unspecialized NSPCs acquire the features of specialized cells, such as neurons and glial cells. Mammalian NSPC produce different lineages of cells at different stages of development. This is modulated by multiple signalling pathways, which act on the activity and expression of neural fate associated genes. The complete mechanisms of NSPC lineage commitment has not been fully characterized but are thought to include intrinsic and extrinsic factors. Moreover, Wnt and Notch signalling pathways have been proven to regulate neural fates. Wnt functions as positive regulator, while Notch plays the opposite role [59, 60].

2 Objectives

Objective 1. To characterise the development of mice lacking DNA repair factor MRI.

Objective 2. To develop complex NHEJ-deficient mouse models.

1. MRI is a recently discovered NHEJ factor possessing adaptor functions, promoting association of several other NHEJ factors to DNA in the presence of DSBs. Through a CRISPR-Cas9 approach, a partial deletion of *Mri exon 2* was induced, resulting in complete gene inactivation in mice. Inactivation of one or multiple NHEJ factors have been shown to cause massively increased levels of apoptosis throughout their developing nervous system [35]. Thus, **the first aim of this project** is to investigate the impact of MRI on neural development in our *Mri*-deficient mouse model. This will be done by comparing the proliferation rates, self-renewal and differentiation ability of NSPC isolated from our *Mri*$^{-/-}$ and WT mice. In addition, growth, body size and fertility of our *Mri* mouse model will be assessed.

2. Single knockout of *Mri* and *Xlf* results in viable mice with no overt phenotype, but combined deficiency of MRI and XLF results in embryonic lethality due to extensive apoptosis in the central nervous system [33]. The fact that these mouse models die as embryos prevents us from studying the MRI.XLF double deficiency *in vivo*. Other embryonically lethal mouse models, such as *Xrcc4*$^{-/-}$, *Lig4*$^{-/-}$, *Xlf*$^{-/-}$*Paxx*$^{-/-}$ and *Xlf*$^{-/-}$*Dna-pkcs*$^{-/-}$, have been shown to be rescued by the inactivation of one or two alleles of *Trp53*, which codes for p53. Based on the phenotypic similarities between *Mri*$^{-/-}$ and *Xlf*$^{-/-}$ or *Paxx*$^{-/-}$, it is speculated that inactivation of *Trp53* can rescue the lethality of *Mri*$^{-/-}$*Xlf*$^{-/-}$ mice. Furthermore, inactivation of both *Paxx* and *Dna-pkcs* results in viable mice. Therefore, it would be interesting to know if combined triple inactivation of *Paxx*, *Dna-pkcs* and *Mri* results in embryonic lethal or viable mice. Thus, **the second aim of this project** is to investigate genetic interaction between MRI, XLF, PAXX, DNA-PKcs and p53 using *Mri*$^{-/-}$*Xlf*$^{-/-}$*Trp53*$^{+/-}$, *Mri*$^{-/-}$*Xlf*$^{-/-}$*Trp53*$^{-/-}$ and *Mri*$^{-/-}$*Paxx*$^{-/-}$*Dna-pkcs*$^{-/-}$ mouse models, which may elucidate hidden roles of the DNA repair factors.

3 Material and methods

3.1 Mouse models

All experiments involving mice were performed according to the protocols approved by the Animal Resources Care Facility of Norwegian University of Science and Technology (NTNU, Norway). *Mri$^{+/-}$* mouse model was custom-generated and described here for the first time. Other mouse models used in this project have previously been described; *Xlf$^{+/-}$* [61], *Dna-pkcs$^{+/-}$* [62], *Paxx$^{+/-}$* [63] and *Trp53$^{+/-}$* [64]. Primer sequences for genotyping and expected amplicons are provided in Appendix A.

3.2 Generation of *Mri^{-/-}* mice

Mri-deficient (*Mri^{-/-}*) mice were generated through a CRISPR/Cas9 gene editing approach in 2017 by Horizon Discovery (Saint Louis, USA) upon request from our lab (the Oksenych group, IKOM, Faculty of Medicine and Health Science, NTNU, Norway). Single-guide RNA (sgRNA) (GGG CTG TCA TCC AAG AGG GGA GG) was designed to target exon 2 coding region of *Mri* in C57BL/6 mice, resulting in a 14 bp deletion. This 14 bp deletion results in a premature stop codon. sgRNA and Cas9 RNA were injected into single cell fertilized embryos and transferred back into pseudo pregnant females for gestation. Live born pups were screened for mutation by PCR, and viable pups were kept and used for breeding.
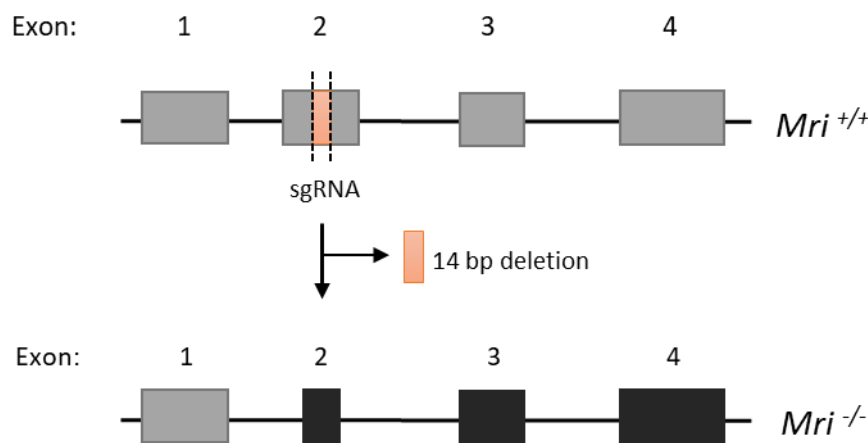
Figure 3.1: Generation of *Mri^{-/-}* mice. Top: Schematic diagram of murine *Mri^{+/+}* locus indicating the target loci in exon 2 for the sgRNA. Bottom: Resulting *Mri^{-/-}* locus lacking part of exon 2, resulting in an early stop codon. Inactivated exons are represented in black.

For the PCR assays, oligonucleotides primers were designed to detect either the original *Mri* loci (428bp and 238bp) or shortened locus corresponding to mutant alleles (414 bp). The primers used to identify mutant mice were designed to detect the deleted 14 bp region of DNA.

3.3 Mouse genotyping

3.3.1 DNA extraction from tissue and the polymerase chain reaction

Two polymerase chain reactions were designed and executed to determine the mouse genotypes. Tail or ear samples from mice were digested overnight at 56°C with 2% Proteinase K (20mg/ml) (Invitrogen™, Carlsbad, California, USA; #AM2548) in DNA lysis solution (10mM Tris pH 9.0, 1 M KCl, 0.4% NP-40, 0.1% Tween 20) in a Thermomixer® comfort (Eppendorf AG, Hamburg, Germany). The following day, samples were boiled for 30 min at 95°C. Debris was spun down at 15000 rpm for 15 minutes. Further, DNA concentration was measured with a Nanodrop® ND-100 Spectophotometer (Thermo Scientific, Waltham, Massachusetts, USA). Samples were diluted to reach a final DNA concentration of ≈ 50 ng/µL. Before preforming the PCR, DNA (≈50 ng) was mixed with ddH$_2$O (11.1 µL), forward primer (0.2 µL), reverse primer (0.2 µL) and Taq 2x (12.5 µL) (Master Mix Kit, New Engand Biolabs® Inc., Ipswitch, Massachusetts, USA; #M0270L). PCR was performed in a 2720 Thermal Cycler (Applied Biosystem™, Foster City, California, USA). First PCR was able to identify bands corresponding to 428 and 414 bps, WT and null allele, respectively. The second PCR (234 bp) was designed to confirm only the presence of the WT allele. Two different agarose gels with GelRed™ Nucleic Acid Gel Stain (diluted from 10 000x stock, Biotium, Fermont, California, USA; #41003) were prepared, one used for 428 bp and another for 234 bp. Primer sequences used for PCR are shown in Table 3.1.

Table 3.1: List of *Mri* PCR primers and their characteristics. (Fw = Forward, Rv = Reverse).

Amplicon length (BP)		Primer sequence	Length (BP)
428 and 414	*Fw*	TCAGGTCTGCCCTACACTGA	20
	Rv	GTGGTGGTGCTTCTCTGTGA	20
234	*Fw*	TCAGGTCTGCCCTACACTGA	20
	Rv	AGAGGGGAGGACCC	14

3.3.2 Electrophoresis

The gels for PCR fragments (e.g., 428 bp and 234 bp) were prepared from 2.5% and 0.7% SeaKem® LE Agarose (Lonza, Basel, Switzerland; #50004), respectively, dissolved in Tris-Borate-EDTA (TBE) buffer (pH 8.4; 89 mM Tris; 89 mM Boric Acid; 2 mM EDTA). The 428 bp gel electrophoresis was performed in TBE buffer at 90 V for 18 hours at 4°C (200 mL gel), while the 234 bp gel electrophoresis was performed in TBE buffer at 124 V for 1 hour and 15 minutes at room temperature (100 mL gel). Sample volume for both gels was 10 μL. Quick-Load® 100 bp DNA Ladder (New England Biolabs® Inc., Ipswich, Massachusetts, USA; #N0467L) and Orange G 5x ≈50 bp (15% glycerol; 0.2% Orange G dye, dH_2O) were used as ladder and tracing dye, respectively. Positive and negative controls, as well as ddH_2O, were used for reliability in all assays. Finally, a ChemiDoc™ MP Imaging System (Bio-Rad, Hercules, California, USA) was used to visualize and capture images of all gels.

3.4 Neural development

3.4.1 Brain isolation and neural stem progenitor cell culture

When grown *in vitro*, neural stem progenitor cells (NSPC) form free-floating globular structures known as neurospheres [65]. Brains were isolated from postnatal day one mice, and cerebellum was removed. The remains of the brain were mechanically disrupted in proliferation medium containing Dulbecco Modified Eagle Medium, Nutrient Mixture F12 (DMEM/F12) (Thermo Fisher Scientific, USA; #11330-057), supplemented with penicillin/streptomycin (1%) (Thermo Fisher, USA; #15140122), B27 without vitamin-A (2%) (Thermo Fischer Scientific, USA; #12587001), EGF (10ng/mL) (PepoTrech, Sweden; #AF-100-15) and bFGF (20ng/mL) (PeproTech, Sweden; #100-18B). As previously described, neurospheres were formed during incubation (37°C, 5% CO_2 and 95% humidity) [65].

3.4.2 Neurosphere passage

Neurospheres were counted and propagated every seven days. The neurospheres were transferred from petri dishes to centrifugation tubes (15 mL). Cells were spun down at 1000rpm at 22°C for 4 minutes and the supernatant was removed. Shortly after, the cell pellet was resuspended in trypsin (3 mL) (Sigma, USA; #T3924) and dissociated mechanically into a single cell suspension. The suspension was incubated at 37°C for 7 minutes. After incubation, the cell suspension was yet again mechanically dissociated and incubated at 37°C for 7 minutes. Proliferation medium (6 mL) was then added to the centrifugation tubes in order to inactivate the trypsin. Then, the suspension was centrifuged at 1000rpm at 22°C for 4 minutes. The supernatant was removed, the cells was resuspended in proliferation medium and passed through a 40 μm strainer (Sigma-Aldrich, USA). Low passage NSCs (P3–P10) were used throughout all the NSPC experiments.

3.4.3 Neural stem progenitor cell proliferation assay

A PrestoBlue™ Cell Viability Assay was used to investigate the NSPCs proliferation rates, following the manufactures instructions. Briefly, dissociated single NSPCs were loaded onto a 96-well-suspension plate at 8000 cells/well in proliferation medium. PrestoBlue™ reagent (10% of well volume) (Thermo Fisher, USA; A13262) was added from day 1 to 7, and incubated (37°C, 5% CO_2 and 95% humidity) for 30 min. The proportion of life cells was estimated by measuring fluorescence intensity using FLUOstar Omega (BMG Labtech, Germany).

3.4.4 Neural stem progenitor cell self-renewal assay

The capacity of neuronal stem cells to maintain their pluripotency *ex vivo* was assessed by determining the number and two-dimensional size of the neurospheres. Dissociated single NSPCs were plated onto 6-well suspension plates containing proliferation medium (day 0). Between days 8 and 10 in culture, images of the entire wells were captured using EVOS microscope (Invitrogen, USA). All the images were analysed for average size using the *ImageJ* (NIH, USA). Only areas between 50 and 1500 pixels were included into the analyses.

3.4.5 Neural stem progenitor cell differentiation assay

Differentiation assay was performed as previously described [60]. On day 0, 25000 single cells were cultured onto 48-well pre-coated plates (30µg/mL poly-D-lysine and 2µg/mL laminin) with differentiation medium containing NeuroBasal A medium (Thermo Fischer Scientific, USA; #10888022) supplemented with penicillin/streptomycin (1%) (Thermo Fisher, USA; #15140122), B27 (2%) (Thermo Fisher Scientific, USA; #17504044), GlutaMAX (1%) (Thermo Fisher Scientific, USA; #35050061) and bFGF (10ng/ml) (PeproTech, Sweden; #100-18B). After 5 days, the differentiated cells were fixed with paraformaldehyde (4%) for 15 min at room temperature. The cells were then permeabilized with 0.1% Triton-X in 1X PBS (300 µL) for 15 minutes, blocked for 45 minutes with 5% BSA, 5% goat gut serum, and 0.1% Triton-X in 1X PBS (500 µL) in room temperature, and incubated overnight at 4°C. The next day, immunocytochemistry was performed using mouse anti-neuron specific β-III tubulin (Tuj1) and rabbit anti-glial fibrillary acidic protein (GFAP) antibodies, to determine neurons and astrocytes after differentiation. All cells were counterstained with 4'6-diamidino-2-phenylindole (DAPI) [60]. Images were visualized utilizing EVOS microscope (Invitrogen, USA). Positive cells were counted manually using ImageJ software and presented as proportion of total cells compared to WT control. Antibodies used in immunocytochemistry are described in Section 3.10.

3.9 Mri.Xlf.Trp53 and Mri.Dna-pkcs.Paxx breeding

Initially, our *Mri* mouse model was crossed with mice heterozygote for *Xlf* and *Trp53* to obtain suitable genotypes for further breeding. Later, *Mri$^{+/-}$Xlf$^{+/-}$Trp53$^{+/-}$* mice were crosses with each other with the goal of obtaining *Mri$^{-/-}$Xlf$^{-/-}$Trp53$^{+/-}$* or *Mri$^{-/-}$Xlf$^{-/-}$Trp53$^{-/-}$* mice. In similar fashion, *Mri$^{+/-}$* mice were crossed with *Paxx$^{+/-}$Dna-pkcs$^{+/-}$* mice in hopes of generating *Mri$^{-/-}$Paxx$^{-/-}$Dna-pkcs$^{-/-}$* mice.

3.10 Antibodies

Information about antibodies used during immunocytochemistry is presented in Table 3.2

Table 3.2: Listed antibodies were used in immunocytochemistry of NSPC. The table indicates antibody host and target, dilutions used, reference (catalogue number), as well as antibody supplier.

Antibody	Host and target, type	Dilution	Reference (Catalogue #)	Supplier
Tuj 1	Mouse anti-neuron specific β-tubulin	1:500	MO15013	R&D Systems, USA
GFAP	Rabbit anti-glial fibrillary acid protein	1:500	Z0334	Dako, Denmark
DAPI	DNA binding	1:1000	62248	Thermo Scientific, USA
Alexa 488	Goat anti-mouse	1:500	A11001	Molecular Probes, USA
Alexa 594	Goat anti-rabbit	1:500	A11032	Molecular Probes, USA

3.11 Statistics

Statistical analysis of NSPC proliferation, self-renewal, and differentiation was performed in GraphPad Prism 8 (La Jolla, California, USA). Unpaired t-test were performed to compare proliferation rates, size and number of neurospheres for self-renewal assay, and proportion of differentiated neurons and astrocytes between WT and *Mri$^{-/-}$* NSPC.

4 Results

4.1 Generation and genotyping of *Mri*^{-/-} mice

To investigate the neurological role of MRI, we generated a mouse model with deletions in the MRI gene coding region on a C57BL/6 background. For this, purified sgRNA and Cas9 RNA were introduced to fertilized oocytes, resulting in a 14 base pair deletion and complete inactivation of the *Mri* gene. *Mri*-deficient mice (*Mri*^{-/-}) organ isolation and breeding was confirmed by PCR screening. For reliability, genomic DNA from WT and mutant mice, and H_2O controls containing no DNA were used in all *Mri* PCR assays. Example of PCR assays performed are presented in Figure 4.1. Overview of PCR programs are presented in Appendix B.
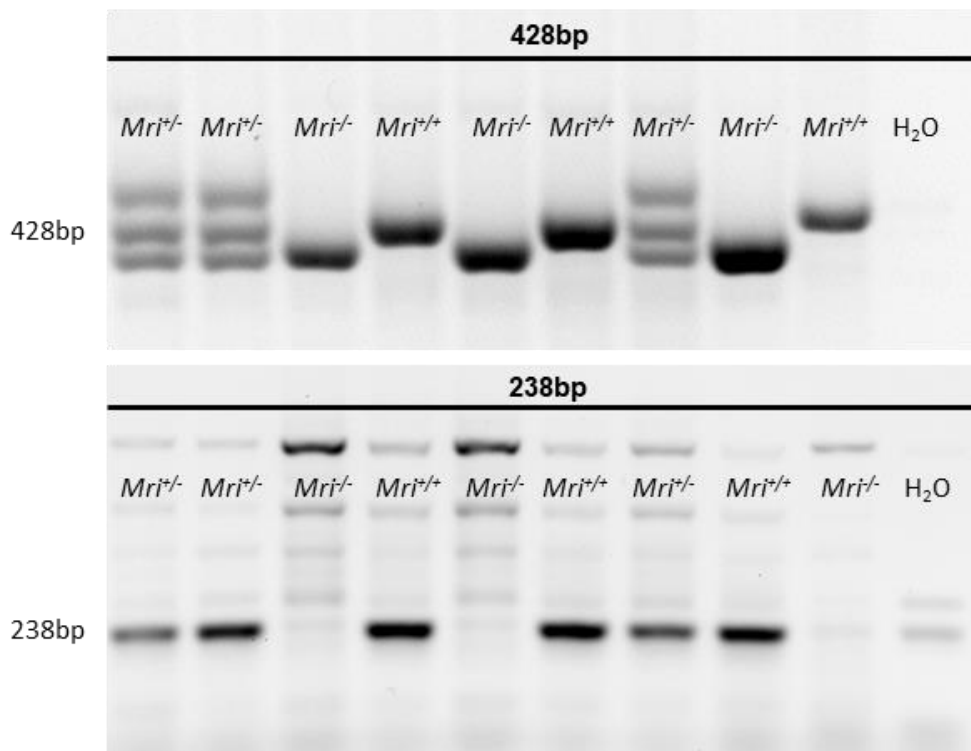
Figure 4.1: PCR-based genotyping strategy reveals the *Mri* WT allele (428 bp) and *Mri* null allele (238 bp). The following samples are presented, from left to right: *Mri*^{+/-}, *Mri*^{+/-}, *Mri*^{-/-}, *Mri*^{+/+}, *Mri*^{-/-}, *Mri*^{+/+}, *Mri*^{+/-}, WT control, *Mri*^{-/-} control, and H_2O.

A total of 93 *Mri* mice were genotyped. Distribution of analysed *Mri*^{+/+}, *Mri*^{+/-} and *Mri*^{-/-} mice, born from *Mri*^{+/-} parents, is presented in Table 4.1.

Table 4.1: Proportion of live born mice. Mendelian distribution (expected, 1:2:1) is shown in the third column. Both parents possessed the *Mri*$^{+/-}$ genotype.

Genotype	Observed	Expected (1:2:1)
Mri$^{+/+}$	17	23.25
Mri$^{+/-}$	45	46.50
Mri$^{-/-}$	31	23.25
Total:	**93**	**93**

In addition, MRI-deficient mice were of similar body size and weight as heterozygous controls (*Mri*$^{+/-}$*Xlf*$^{+/-}$*Paxx*$^{+/-}$) (Fig. 4.2 and 4.3).

Figure 4.2: Examples of age and gender-matched heterozygous control (*Mri*$^{+/-}$ *Xlf*$^{+/-}$*Paxx*$^{+/-}$) and *Mri*$^{-/-}$ mice (2 months old females).
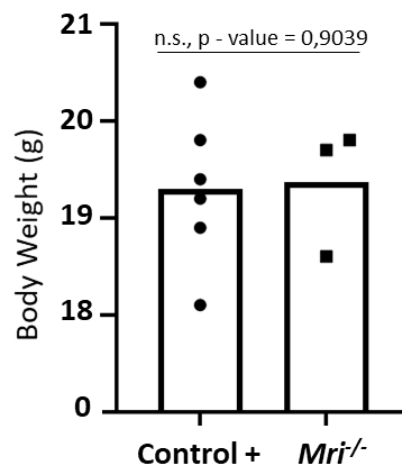
Figure 4.3: The average weight of thirty-day-old mice in grams. p-value was calculated using unpaired t-test.
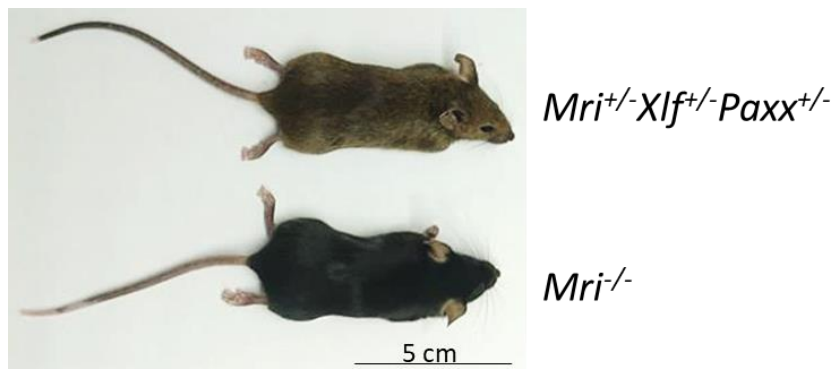
4.2 Proliferation of the NSPC

Other studies have shown that single knockout of NHEJ DNA repair genes, e.g. *Xrcc4*, results in impaired nervous system development in mice [66]. To investigate the impact of MRI on the developing nervous system, we decided to isolate NSPC from *Mri*$^{+/+}$ and *Mri*$^{-/-}$ postnatal day one mice and study the NSPCs proliferation capacity *in vitro*. Proliferation ratios of the neurospheres were assessed using PrestoBlue™ Cell Viability Assay. The average proliferation rate of *Mri*$^{-/-}$ neurospheres was significantly reduced compared to that of WT neurospheres, p = 0,0043 (Fig. 4.4).
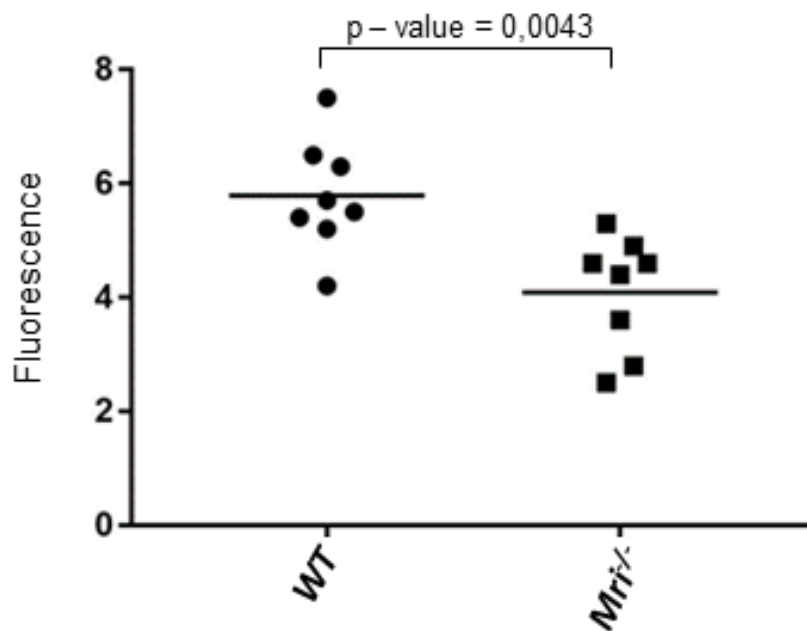
Figure 4.4: Comparison of the proliferation ratios between WT (*Mri*$^{+/+}$) and *Mri*$^{-/-}$ NSPC. Data show the 168h proliferation (day 1 to day 7 in culture) normalized to wild type at 0 h average. Dots account for the value of 2 clones per genotype and 4 repeats of each experiment (n = 8). p-value was calculated using unpaired t-test, and horizontal bars represent the average.

4.3 Self-Renewal of the NSPC

To analyse the capacity of the neurospheres to remain as NSPCs throughout cell divisions and numerous propagations (self-renewal capacity), equal amount of single NSPCs were plated and the number of neurospheres formed after 8 to 10 days in culture was counted. In addition, to estimate the growth rate of cells inside the neurospheres, single NSPC (10^4 cells) were plated kept in culture for 8 days. On the 8th day, the images of the cells were taken using EVOS microscope, and the computer software *ImageJ* was used to determine the number and the size of the neurospheres. Inactivation of *Mri* resulted in neurospheres numbers indistinguishable from WT (*Mri$^{+/+}$*) controls, p = 0,7254 (Fig. 4.5). In addition, inactivation of *Mri* resulted in neurospheres with similar diameter as WT (*Mri$^{+/+}$*) controls, p = 0,4915 (Fig. 4.6). Examples of EVOS images analysed by ImageJ are presented in Figure 4.7.
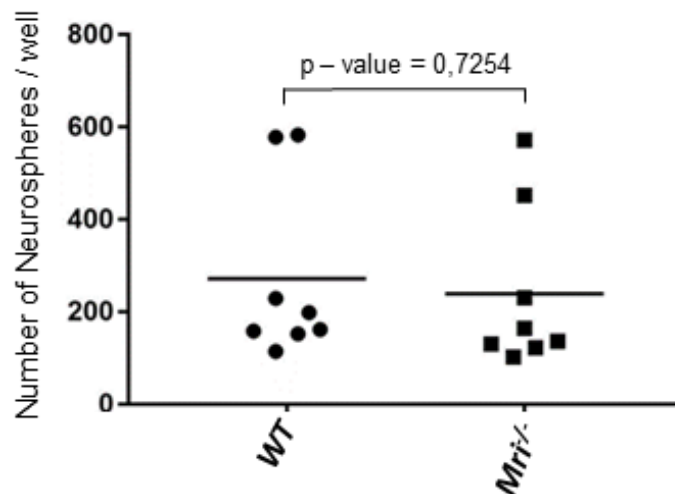
Figure 4.5: Comparison of the neurosphere number formed after 8 – 10 days in culture between WT and *Mri$^{-/-}$* NSPC. Dots account for the value of 2 clones per genotype and 4 repeats of each experiment (n = 8). p-value was calculated using unpaired t-test. Horizontal bar represents the average.
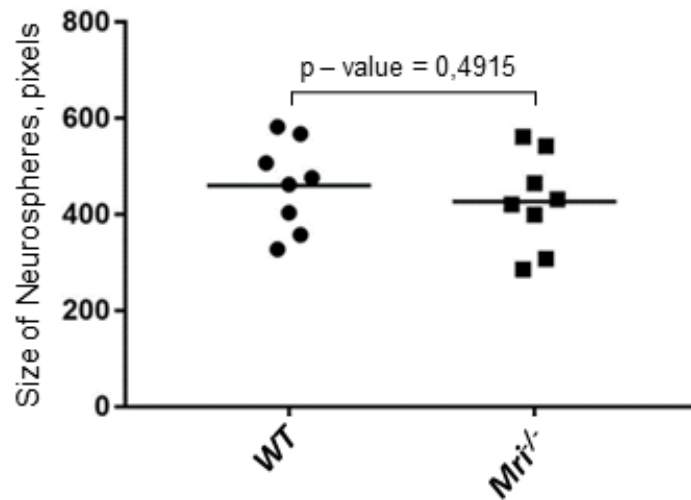
Figure 4.6: Comparison of the neurosphere size formed after 8 – 10 days in culture between WT (*Mri*$^{+/+}$) and *Mri*$^{-/-}$ NSPC. Dots account for the value of 2 clones per genotype and 4 repeats of each experiment (n = 8). p-value was calculated using unpaired t-test. Horizontal bar represents the average.
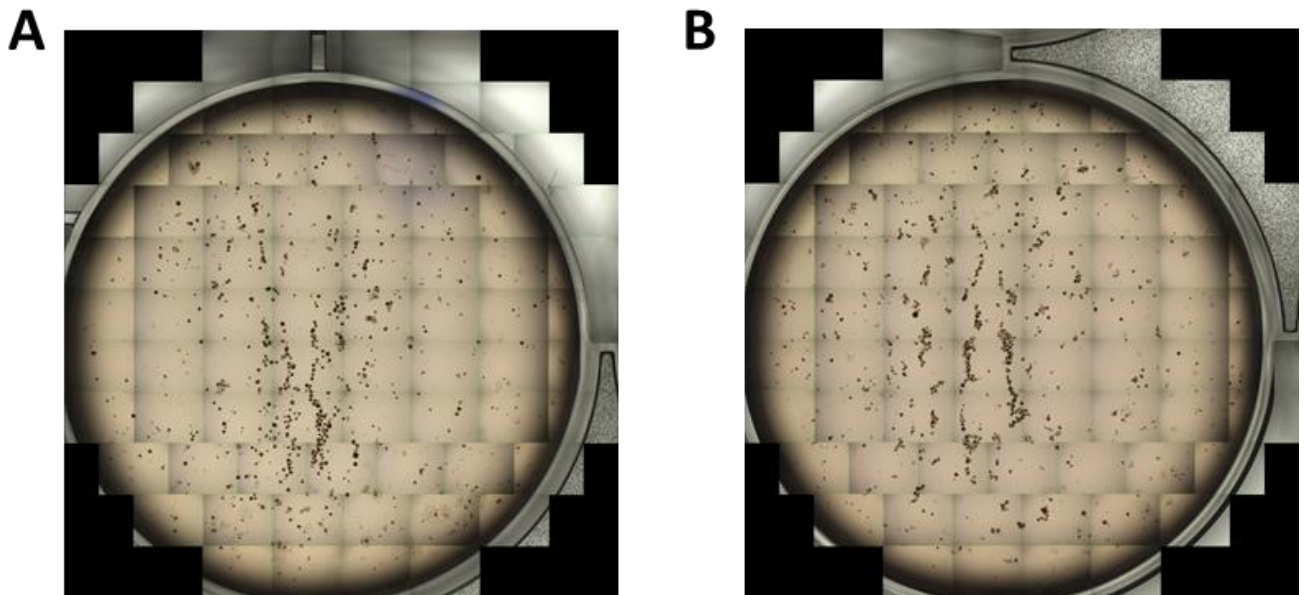
Figure 4.7: Examples of images collected using the EVOS microscope. The images represent neurospheres cultured for 8 – 10 days. **A**) Example of *Mri*$^{+/+}$ neurospheres. **B**) Example of *Mri*$^{-/-}$ neurospheres.

4.4 Differentiation

To determine whether MRI affect the differentiation capacity of the neurospheres, single NSPCs were plated on pre-coated petri dishes and cultured with differentiation medium for 5 days. Neuronal and glial lineages were identified by immunolabeling using a marker for early neurons (Tuj1), and for astrocytes (GFAP), as described previously [60]. Inactivation of *Mri* did not affect early neuronal differentiation nor the differentiation of glial lineage cells, p = 0,798 and p = 0,598 respectively (Fig. 4.8 and Fig. 4.9). Positive cells were divided by total cells. Statistical analysis (unpaired t-test) was performed in GraphPad Prism. Examples of the immunocytochemistry against Tuj1 and GFAP are presented in Figure 4.10.
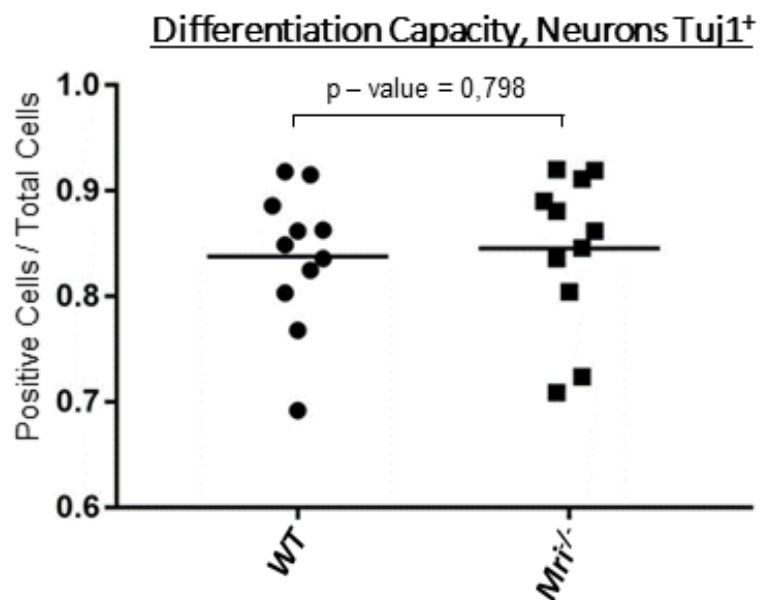
Figure 4.8: Comparison of the neuronal differentiation capacity between WT (*Mri*$^{+/+}$) and *Mri*$^{-/-}$ NSPC. Dots account for 3 or 4 clones per genotype and 3 repeats of each experiment (n = 11). Horizontal bar represents the average.
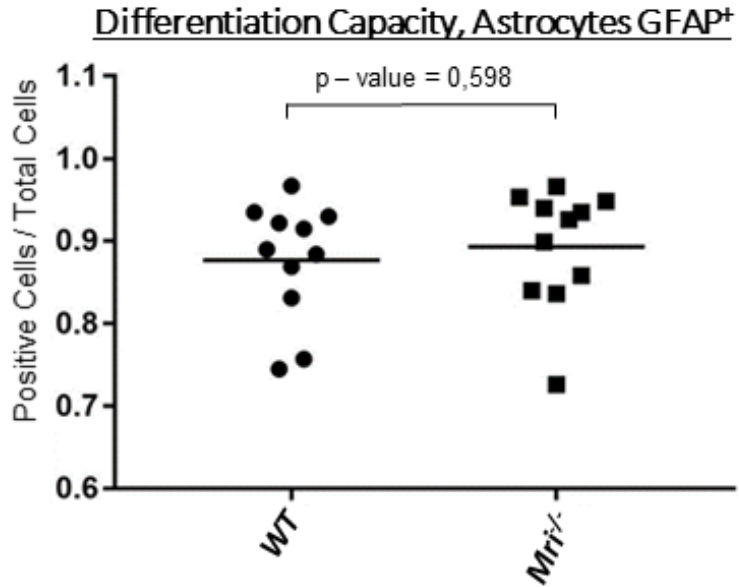
Figure 4.9: Comparison of the glial differentiation capacity between WT (*Mri*^{+/+}) and *Mri*^{-/-} NSPC. Dots account for 3 or 4 clones per genotype and 3 repeats of each experiment (n = 11). Horizontal bar represents the average.
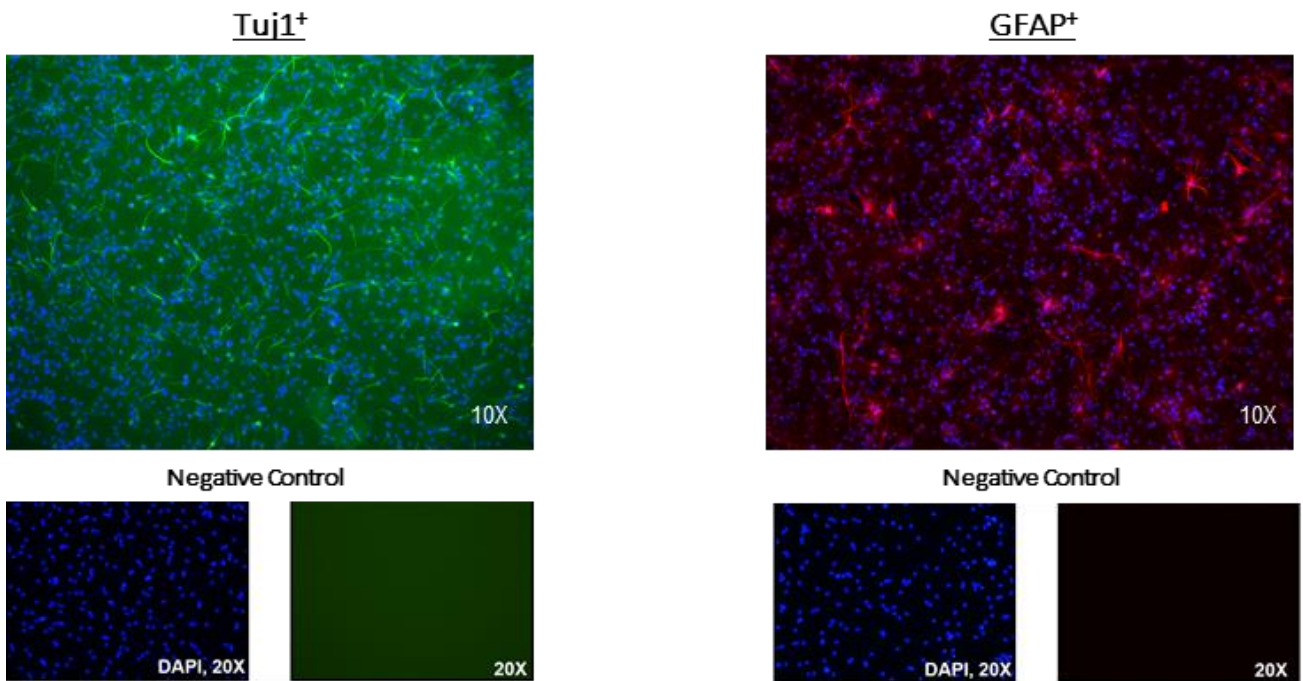
Figure 4.10: Examples of the immunocytochemistry against Tuj1 and GFAP. Left panel, Tuj1+ cells are in green. Right panel, GFAP+ cells are in red. Both immunocytochemistries were counterstained with DAPI (blue). Negative controls were performed without the primary antibody.

4.5 Mri.Xlf.Trp53 breeding

According to previous studies, combined deficiency of XLF and PAXX, XLF and DNA-PKcs, and MRI and XLF resulted in late embryonic lethality (E15.5) in mice, complicating the ability to investigate double deficiency *in vivo* [24, 33, 34]. However, previous findings show that inactivation of one or both alleles of *Trp53* (encoding p53) partially rescue the lethality of *Xlf$^{-/-}$Paxx$^{-/-}$* mice. To investigate if deletion or haploinsufficiency of the *Trp53* gene can rescue XLF and MRI combined deficiency, *Mri$^{+/-}$Xlf$^{+/-}$Paxx$^{+/-}$Trp53$^{+/-}$* mice were intercrossed with each other with the goal of obtaining *Mri$^{-/-}$Xlf$^{-/-}$Trp53$^{+/-}$* or *Mri$^{-/-}$Xlf$^{-/-}$Trp53$^{-/-}$* mice. So far, 44 pups were screened in total. Distribution of analysed mice is presented in Table 4.2. Due to embryonic lethality, no viable *Mri$^{-/-}$Xlf$^{-/-}$Trp53$^{+/+}$* mice were expected. Examples of PCR assays performed are presented in Figure 4.11. No *Mri$^{-/-}$Xlf$^{-/-}$Trp53$^{+/-}$* or *Mri$^{-/-}$Xlf$^{-/-}$Trp53$^{-/-}$* mice were identified during the screening process. Strikingly, at least two mice in this breeding were found dead during the first three weeks of live and removed by the core facility staff before they could be analysed.

Table 4.2: All possible *Mri.Xlf.Trp53* genotypes of pups and the number of pups identified for each genotype. In total, 44 pups were screened. Genotypes in bold indicate desired genotypes to investigate MRI and XLF double deficiency *in vivo*.

Possible Genotypes	Pups
Mri$^{+/+}$Xlf$^{+/+}$Trp53$^{+/+}$	-
Mri$^{+/+}$Xlf$^{+/+}$Trp53$^{+/-}$	3
Mri$^{+/+}$Xlf$^{+/+}$Trp53$^{-/-}$	1
Mri$^{+/+}$Xlf$^{+/-}$Trp53$^{+/+}$	3
Mri$^{+/+}$Xlf$^{+/-}$Trp53$^{+/-}$	2
Mri$^{+/+}$Xlf$^{+/-}$Trp53$^{-/-}$	1
Mri$^{+/+}$Xlf$^{-/-}$Trp53$^{+/+}$	-
Mri$^{+/+}$Xlf$^{-/-}$Trp53$^{+/-}$	2
Mri$^{+/+}$Xlf$^{-/-}$ Trp53$^{-/-}$	-
Mri$^{+/-}$Xlf$^{+/+}$Trp53$^{+/+}$	1
Mri$^{+/-}$Xlf$^{+/+}$Trp53$^{+/-}$	8
Mri$^{+/-}$Xlf$^{+/+}$Trp53$^{-/-}$	2
Mri$^{+/-}$Xlf$^{+/-}$Trp53$^{+/+}$	3
Mri$^{+/-}$Xlf$^{+/-}$Trp53$^{+/-}$	5
Mri$^{+/-}$Xlf$^{+/-}$Trp53$^{-/-}$	1
Mri$^{+/-}$Xlf$^{-/-}$Trp53$^{+/+}$	1
Mri$^{+/-}$Xlf$^{-/-}$Trp53$^{+/-}$	1
Mri$^{+/-}$Xlf$^{-/-}$ Trp53$^{-/-}$	1

Possible Genotypes	Pups
Mri$^{-/-}$Xlf$^{+/+}$Trp53$^{+/+}$	-
Mri$^{-/-}$Xlf$^{+/+}$Trp53$^{+/-}$	2
Mri$^{-/-}$Xlf$^{+/+}$Trp53$^{-/-}$	2
Mri$^{-/-}$Xlf$^{+/-}$Trp53$^{+/+}$	2
Mri$^{-/-}$Xlf$^{+/-}$Trp53$^{+/-}$	1
Mri$^{-/-}$Xlf$^{+/-}$Trp53$^{-/-}$	2
Mri$^{-/-}$Xlf$^{-/-}$Trp53$^{+/+}$	-
Mri$^{-/-}$Xlf$^{-/-}$Trp53$^{+/-}$	-
Mri$^{-/-}$Xlf$^{-/-}$ Trp53$^{-/-}$	-
Total	44
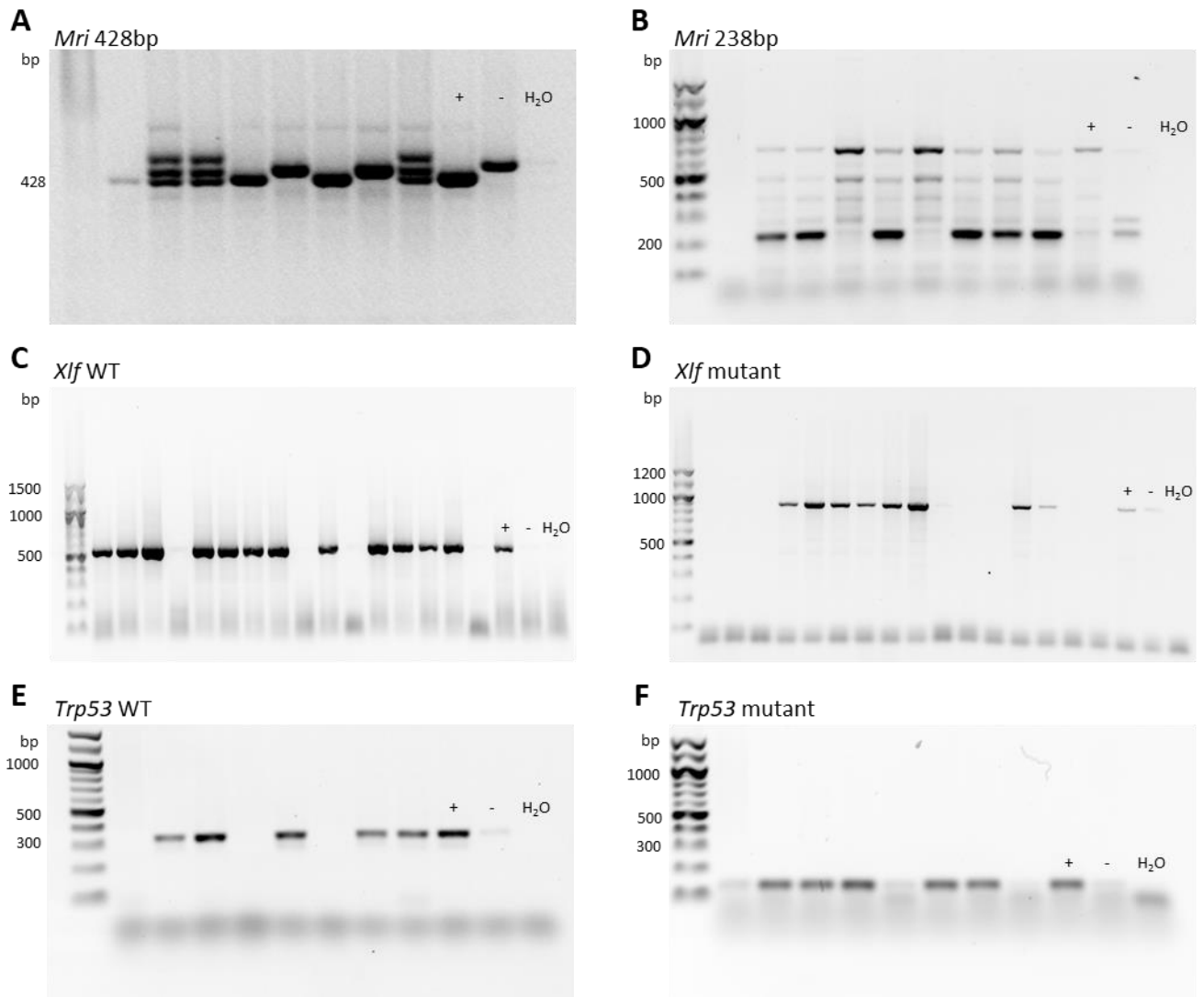
Figure 4.11: Examples of PCR analysis for *Mri, Xlf and Trp53* with indicated controls; "+" indicates WT allele of corresponding gene (positive control), and "-" indicate mutant allele of corresponding gene. A) *Mri* 428bp. The lowest band corresponds to the mutant allele (414bp), whereas bands in the middle correspond to WT allele (428bp). Samples with multiple bands are heterozygote. B) *Mri* 238bp. The lower bands correspond to the WT allele (238bp), and the remaining bands are background. C) *Xlf* WT. Bands correspond to the *Xlf* WT allele (650bp). D) *Xlf* mutant. Bands correspond to the *Xlf* mutant allele (950bp). E) *Trp53* WT. Bands correspond to the WT allele (321bp). F) *Trp53* mutant. Bands correspond to the mutant allele (150bp).

4.6 Mri.Paxx.Dna-pkcs breeding

As described in Section 4.5, double deficiency of XLF and either PAXX, or DNA-PKcs, or MRI results in embryonic lethality in mice [24, 33, 34]. However, combined deficiency of PAXX and DNA-PKcs results in viable mice. To further enlighten the genetic interaction between the NHEJ factors, $Mri^{+/-}$ mice were crossed with $Paxx^{+/-}Dna\text{-}pkcs^{+/-}$, resulting in $Mri^{+/-}Paxx^{+/-}Dna\text{-}pkcs^{+/-}$ mice. These mice were intercrossed in order to generate $Mri^{-/-}Paxx^{-/-}Dna\text{-}pkcs^{-/-}$ mice. So far, 45 pups were screened in total. Distribution of analysed mice is presented in Table 4.3. Examples of PCR assays performed are presented in Figure 4.12. No $Mri^{-/-}Paxx^{-/-}Dna\text{-}pkcs^{-/-}$ mice were identified during the screening process.

Table 4.3: All possible *Mri.Paxx.Dna-pkcs* genotypes of pups and the number of pups identified for each genotype. In total, 45 pups were screened. Genotypes in bold indicate desired genotypes to investigate combined MRI, PAXX and DNA-PKcs deficiency *in vivo*.

Possible genotypes	Pups
$Mri^{+/+}Paxx^{+/+}Dna\text{-}pkcs^{+/+}$	-
$Mri^{+/+}Paxx^{+/+}Dna\text{-}pkcs^{+/-}$	-
$Mri^{+/+}Paxx^{+/+}Dna\text{-}pkcs^{-/-}$	-
$Mri^{+/+}Paxx^{+/-}Dna\text{-}pkcs^{+/+}$	2
$Mri^{+/+}Paxx^{+/-}Dna\text{-}pkcs^{+/-}$	5
$Mri^{+/+}Paxx^{+/-}Dna\text{-}pkcs^{-/-}$	-
$Mri^{+/+}Paxx^{-/-}Dna\text{-}pkcs^{+/+}$	1
$Mri^{+/+}Paxx^{-/-}Dna\text{-}pkcs^{+/-}$	4
$Mri^{+/+}Paxx^{-/-}Dna\text{-}pkcs^{-/-}$	2
$Mri^{+/-}Paxx^{+/+}Dna\text{-}pkcs^{+/+}$	-
$Mri^{+/-}Paxx^{+/+}Dna\text{-}pkcs^{+/-}$	3
$Mri^{+/-}Paxx^{+/+}Dna\text{-}pkcs^{-/-}$	1
$Mri^{+/-}Paxx^{+/-}Dna\text{-}pkcs^{+/+}$	3
$Mri^{+/-}Paxx^{+/-}Dna\text{-}pkcs^{+/-}$	9
$Mri^{+/-}Paxx^{+/-}Dna\text{-}pkcs^{-/-}$	1
$Mri^{+/-}Paxx^{-/-}Dna\text{-}pkcs^{+/+}$	1
$Mri^{+/-}Paxx^{-/-}Dna\text{-}pkcs^{+/-}$	6
$Mri^{+/-}Paxx^{-/-}Dna\text{-}pkcs^{-/-}$	1

$Mri^{-/-}Paxx^{+/+}Dna\text{-}pkcs^{+/+}$	1
$Mri^{-/-}Paxx^{+/+}Dna\text{-}pkcs^{+/-}$	1
$Mri^{-/-}Paxx^{+/+}Dna\text{-}pkcs^{-/-}$	-
$Mri^{-/-}Paxx^{+/-}Dna\text{-}pkcs^{+/+}$	-
$Mri^{-/-}Paxx^{+/-}Dna\text{-}pkcs^{+/-}$	2
$Mri^{-/-}Paxx^{+/-}Dna\text{-}pkcs^{-/-}$	-
$Mri^{-/-}Paxx^{-/-}Dna\text{-}pkcs^{+/+}$	-
$Mri^{-/-}Paxx^{-/-}Dna\text{-}pkcs^{+/-}$	2
$Mri^{-/-}Paxx^{-/-}Dna\text{-}pkcs^{-/-}$	-
Total	45
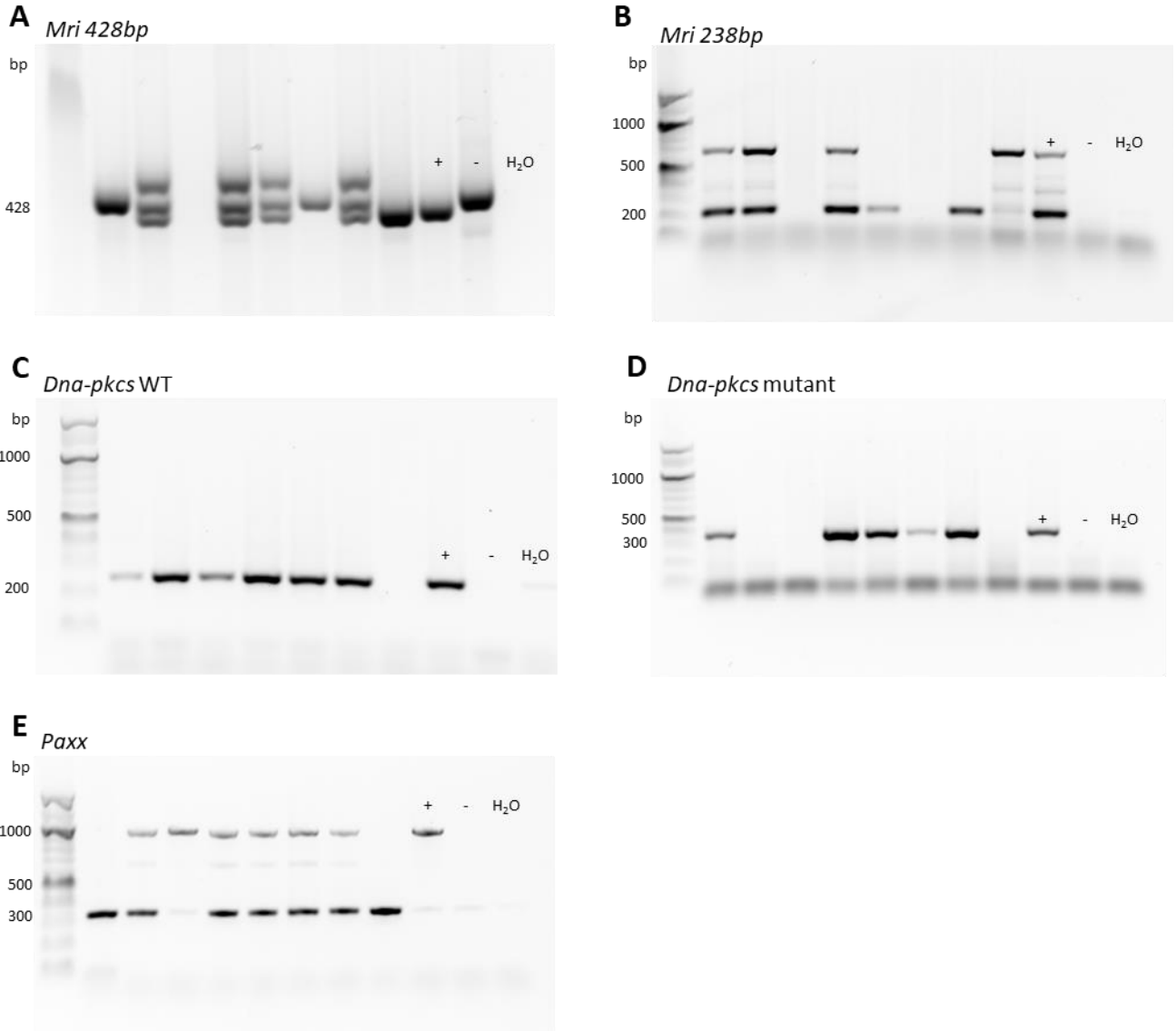
Figure 4.12: Examples of PCR analysis for *Mri, Paxx and Dna-pkcs* with indicated controls; "+" indicates WT allele, and "-" indicates mutant allele. A) *Mri* 428bp. The lowest band corresponds to the mutant allele (414bp), whereas bands in the middle correspond to WT allele (428bp). Samples with multiple bands are heterozygote. B) *Mri* 238bp. The lower bands correspond to the WT allele (238bp), and the remaining bands are background. C) *Dna-pkcs* WT. Bands correspond to *Dna-pkcs* WT allele (250bp). D) *Dna-pkcs* mutant. Bands correspond to mutant allele (427bp). E) *Paxx*. The upper band correspond to the WT allele (965bp), whereas the lower band correspond to the mutant allele (either 329, 312, or 295bp). Samples with two bands are heterozygote.

5 Discussions

5.1 Generation and growth of *Mri* deficient mice

Genetically engineered mice generally represent valuable models for the function of DDR factors and have been used extensively in the study of NHEJ factors. Inactivation of most of the known NHEJ factor genes in mice leads to immunodeficiency [14]. Here we utilized our own custom generated *Mri* knockout mouse model to analyse the effect of the accessory NHEJ factor MRI on NSPC development. To obtain knockout *Mri* mice, we deleted part of the *Mri* exon 2 coding region using the CRISPR/Cas9 approach.

Inactivation of one or both *Mri* alleles resulted in viable and fertile mice with indistinguishable phenotype from WT littermates. As Table 4.1 show, the pups from *Mri*$^{+/-}$ parents were born at nearly-expected Mendelian proportions (1 : 2 : 1); 17 *Mri*$^{+/+}$, 45 *Mri*$^{+/-}$ and 31 *Mri*$^{-/-}$ mice. Furthermore, thirty-day-old *Mri*$^{-/-}$ mice were of similar size compared to WT littermates. The phenotype of MRI deficient mice, as well as that of XLF and PAXX deficient mice [33], is relatively mild when compared with core-NHEJ factors deficient mice, e.g. lacking XRCC4 and LIG4 [35]. The mild phenotypes of *Mri*$^{-/-}$, *Xlf*$^{-/-}$ and *Paxx*$^{-/-}$ mice has mainly been explained by functional redundancy between the accessory NHEJ factors, as studies have shown that mice with multiple accessory NHEJ factor deficiency possess more detrimental phenotypes [24, 34]. All in all, our results show that inactivation of the *Mri* coding gene alone does not affect the fertility, growth and size in mice. This is in line with observations done by other researchers last year (2018) [14].

5.2 Neural stem cell cultures

Stem cells are remarkable cells that exhibit the ability to proliferate, undergo self-renewal and differentiate, thus having a crucial role for maintaining tissue homeostasis. Isolation of NSPC from their original microenvironment and subsequent sub culturing *in vitro*, as performed in this study, allows for a more focused study of the biological mechanisms in these cells. Moreover, such assays have been extensively utilized by researchers as a valuable tool for isolating and understanding the biology of embryonic and adult CNS stem cells. Here this cell culture system is used as a tool to study neurogenesis and their distinct stages, particularly cell proliferation, self-renewal and differentiation in $Mri^{+/+}$ and $Mri^{-/-}$ mice.

Various aspects must be considered when working with NSPC *in vitro*. To ensure that the NSPC maintain their native characteristics, they must be cultured in a model that closely resemble that of the CNS. This includes cultivation in serum-free medium with the additions of mitogens, e.g. epidermal growth factors (EGFs). Second, to avoid premature differentiation, NSPC should be grown under non-adherent conditions [67, 68]. Finally, before assessing the ability of NSPC to undergo neurogenesis, cells must be propagated as secondary and tertiary cultures to ensure that the isolated CNS cells in fact are NSPC [69]. For this project, postnatal day three (P3) pups were originally chosen as cell donors, but due to the cell inability to propagate as neurospheres a new litter of postnatal day one (P1) pups had to be used. This is probably due to that too high of a percentage of the NSPC in P3 pups had already started to differentiate. Other studies have shown similar tendencies [70].

Even though the neurosphere assay is widely used in research, it does have some limitations. First, NSPC are sensitive to mitogen concentrations and number of passages. Researchers have found that the cells should not be propagated more than 10 times, limiting their usability. Rapidly dividing cells and unlimited expansion of cultures can induce loss of proliferative capacity, as high enough number of passages can lead to loss of stemness property [69, 71, 72]. In 2002, Morshed *et al.* found that long term passaged neurospheres can arise in conditions without growth factors, acquiring tumour-like phenotypes [71]. Moreover, other studies have proven that long term culturing (more than 10 propagations) of NSPC as neurospheres results in a decreased ability to differentiate into neurons, as well as a reduction in telomere length and increased chromosomal instability of the NSPC [72]. Thus, only neurospheres cultured for short periods, i.e. 3 – 10 weeks, were used during this project. Second, NSPC are sensitive the mechanism of neurosphere dissociation, e.g. enzymatic digestion or mechanical disruption, which must be carefully performed to avoid excessive cell death [70].

5.3 NSPC proliferation

The evidence of NSPC formation and proliferation in adult mammalian brain was first discovered in 1965. During the early stage of neurodevelopment, there is a high rate of proliferation, which increase the likelihood of DNA damages arising from the DNA replicating machinery. Therefore, during neurogenesis, NHEJ is important to maintain genomic stability of the NSPCs. Here, by the use of a PrestoBlue cell viability assays, I have demonstrated that the NHEJ factor MRI support cellular proliferation during mammalian neurogenesis. Reduced proliferation is most probably caused by programmed cell death via the p53-dependent pathway due to increased DSBs and insufficient DNA repair. This statement is supported by previous studies [33, 35].

PrestoBlue assays are based on resazurin which is a cell permeable redox indicator that is used for monitoring viable cell numbers. In viable cells, with active metabolism, resazurin is metabolically reduced to resorufin within the mitochondria. This reduction causes PrestoBlue to convert from a non-fluorescent form to a fluorescent form [73]. The conversion from resazurin to resorufin is proportional to the number of metabolically active cells and can thus be quantitatively measured using fluorescence measurements. When assessing the cell viability of the NSPC cells must be in a single-cell suspension prior to any experimentation, as aggregates may shield cells from the resazurin resulting in lower fluorescence signal. In the future, experimentally investigating if $Mri^{-/-}$ NSPC have no impaired mitochondrial metabolism would support the reliability of the PrestoBlue results.

As previously explained, $Mri^{-/-}$ mice are viable and fertile mice with indistinguishable phenotype from WT littermates. Behaviour studies would be needed to address whether or not the decreased proliferation rates of $Mri^{-/-}$ NSPC have any negative effects on the $Mri^{-/-}$ mice.

5.4 NSPC self-renewal

The concept of self-renewal is defined as the capability of a single cell to generate a clone. In the case of the neurosphere assay, self-renewal is the ability of a single cell to form subcloned neurospheres. The capacity for self-renewal is vital because it allows a stem cell population to perpetuate and is the most crucial indicator of stemness. The capacity of neurospheres to remains as NSPC throughout cell division was quantified by counting the number of neurospheres formed after 8 – 10 days. No difference between $Mri^{+/+}$ and $Mri^{-/-}$ neurosphere numbers was detected. In addition, the cell growth rate within the neurospheres was estimated by measuring the width of the neurospheres after 8 – 10 days in culture. As the results show, inactivation of Mri had no effect on neurosphere size when compared to WT. Thus, MRI deficient NSPCs are as able to maintain their pluripotency as WT NSPCs *in vitro*.

When assessing the number and size of formed neurospheres, it is important that the cell plating density does not surpass 4000 cells per well so that one ensures that individual neurospheres are clonally derived and not the result of cell clumping. When examining the neurospheres it is important to make sure that the neurospheres are uniformly spaced in the wells. This is important to make sure that ImageJ more easily can differentiate the individual neurosphere, thus resulting in more precise calculation of the number of neurospheres and their size.

Neurospheres consists of hundreds to thousands of cells, and the number of cells is correlated with the size of the neurosphere (usually ranging between 100 and 200 mm of diameter), and with the days of *in vitro* culture. For this project, neurosphere size was used to assess self-renewal ability. On the other hand, due to the fact that the size of the spheres correlates with the number of cells, the increase in cell number between successive passages can additionally be used to quantify the proliferation potential of NSPC [74]. However, it is important to note that this does not contradict our proliferations results, as these cells were grown as neurospheres, not single cells, and the neurospheres were grown for longer periods of time under other conditions. This was further explained in Section 1.4.

5.5 NSPC differentiation

After the removal of mitogens, NSPC may differentiate into different cell types, namely neurons and astrocytes [75, 76]. Different markers can be used to detect and differentiate between the cell types in culture [77, 78]. To determine whether MRI affect the differentiation capacity of neurospheres, neuronal and glial lineages were identified and analysed using markers for early neurons (Tuj1) and for astrocytes (GFAP). For this project, I show that NSPC dissociated from neurospheres produced both neurons and astrocytes after 5 days culturing. No significant difference between the ratio of $Mri^{+/+}$ and $Mri^{-/-}$ positive neurons (Tuj1 positive) were observed. In similar fashion, there was neither no significant difference between the ratio of $Mri^{+/+}$ and $Mri^{-/-}$ positive astrocytes (GFAP positive). Thus, MRI is dispensable for the differentiation of NSPC.

5.6 Mri.Xlf.Trp53 and Mri.Paxx.Dna-pkcs breeding

Although forty-four *Mri.Xlf.Trp53* mice were analysed during this project, no *Mri^{-/-}Xlf^{-/-}Trp53^{+/-}* nor *Mri^{-/-}Xlf^{-/-}Trp53^{-/-}* mice were identified. The genes encoding for MRI, XLF and p53 are all located on separate chromosomes (murine chromosome 6, 1, and 11, respectively), allowing for independent assortment of alleles. It should therefore be possible to achieve triple knockouts and *Mri^{-/-}Xlf^{-/-}Trp53^{+/-}* mice, given that these mice are viable. In similar fashion, forty-five *Mri.Paxx.Dna-pkcs* mice were analysed, and no *Mri^{-/-}Paxx^{-/-}Dna-pkcs^{-/-}* mice were found. *Mri*, *Paxx*, and *Dna-pkcs* are all located on different chromosomes (murine chromosome 6, 2 and 16, respectively). It should therefore be possible to get *Mri^{-/-}Paxx^{-/-}Dna-pkcs^{-/-}* mice, given that the triple deficient mice are viable. The probability of getting *Mri^{-/-}Xlf^{-/-}Trp53^{+/-}* or *Mri^{-/-}Paxx^{-/-}Dna-pkcs^{-/-}* mice, when crossing triple heterozygote mice of desired genotype, is 3/64 (about 1 in 21). Therefore, before any conclusion about viability can be made, more mice need to be analysed. It is very unfortunate that the two dead pups from the *Mri.Xlf.Trp53* breeding were not analysed, as they might have possessed the desired genotype I was searching for. If no *Mri^{-/-}Xlf^{-/-}Trp53^{+/-}* or *Mri^{-/-}Paxx^{-/-}Dna-pkcs^{-/-}* mice are detected after excessive genotyping, one could start analysing embryos to screen for the desired genotypes and determine at which embryonical day the mice experience lethality.

Other studies have shown that neural apoptosis and embryonic lethality can be rescued by crossing XRCC4-, Lig4-deficient, and XLF/PAXX double-deficient mice into a *p53* knockout background. Although the mice were viable, they were much smaller compared to WT littermates and were prone to B cell lymphomas due to unresolved RAG-induced DSBs and translocations [39]. Due to the phenotypic similarities between *Xlf^{-/-}Paxx^{-/-}* and *Mri^{-/-}Xlf^{-/-}*, one would speculate that the same goes for *Xlf^{-/-}Paxx^{-/-}Trp53^{+/-}* and *Mri^{-/-}Xlf^{-/-}Trp53^{+/-}* mice as well. If *Mri^{-/-}Xlf^{-/-}Trp53^{+/-}* mice would prove to be viable, it would allow for *in vivo* studies of functional interactions between MRI and XLF in double deficient mice and would help to elucidate the physiological roles of both MRI and XLF. Moreover, PAXX and DNA-PKcs combined deficient mice are viable. If *Mri^{-/-}Paxx^{-/-}Dna-pkcs^{-/-}* mice are viable, it would allow for *in vivo* studies of MRI, PAXX and DNA-PKcs triple deficient mice. Further investigation of overlapping and non-overlapping functions among MRI and other NHEJ factors, such as XLF, PAXX and DNA-PKcs, would help deepen our current understanding of the function of MRI, and thus NHEJ in general.

6 Conclusions

PCR analysis indicated that applied CRISPR-Cas9 inactivation of *Mri* coding gene was able to produce both *Mri$^{+/-}$* and *Mri$^{-/-}$* mice. Neither deficiency nor haploinsufficiency for *Mri* affected the size, growth and fertility in *Mri$^{+/-}$* or *Mri$^{-/-}$* mice. Ergo, MRI-deficient mice are phenotypic indistinguishable from WT mice. Additionally, based on NSPC experiments, *Mri$^{-/-}$* neurospheres showed comparable self-renewal ability as WT neurospheres. Thus, MRI deficient NSPCs are fully capable of maintaining their pluripotency. Finally, immunohistochemistry showed that MRI does not affect the differentiation capacity of NSPCs. However, PrestoBlue cell viability assay showed impaired proliferation rates of *Mri$^{-/-}$* NSPCs, indicating that MRI support NSPC proliferation. The reduced proliferation of *Mri$^{-/-}$* NSPC might be a result of increased apoptosis mediated by p53. Based on all the presented findings, I can conclude that MRI is a non-essential NHEJ factor for the growth and fertility of mice, with comparable phenotypes to WT and *Paxx$^{-/-}$* mice. Furthermore, it is concluded that MRI-deficient NSPCs are fully capable of maintaining their pluripotency and ability to differentiate into neuronal and glial lineages. However, it is here concluded that MRI does support the proliferation of NSPCs.

Among the 44 *Mri.Xlf.Trp53* mice analysed, no *Mri$^{-/-}$Xlf$^{-/-}$Trp53$^{+/-}$* nor *Mri$^{-/-}$Xlf$^{-/-}$Trp53$^{-/-}$* mice were identified. More mice must be analysed before any conclusion about viability of these mouse models can be made. If these mice prove to be viable, it would allow for *in vivo* studies of *Mri$^{-/-}$Xlf$^{-/-}$* mice. In addition, among the 45 *Mri.Paxx.Dna-pkcs* mice analysed, no *Mri$^{-/-}$Paxx$^{-/-}$Dna-pkcs$^{-/-}$* mice were found. If triple deficient mice are viable, it would allow for *in vivo* study of the overlapping functions and interactions between MRI, PAXX and DNA-PKcs. Investigation of the overlapping and non-overlapping functions between these accessory NHEJ factors would further enlighten our current understandings of the functional interaction between these proteins and enhance our perceptions of NHEJ.

7 References

1. Parkin, J. and B. Cohen, *An overview of the immune system.* Lancet, 2001. **357**(9270): p. 1777-89.
2. Murphy, K.a.W., Casey, *Janeway's Immunobiology*, ed. 9. 2017: Garland Science, Taylor & Francis Group, LLC. p. 1 - 77.
3. LeBien, T.W. and T.F. Tedder, *B lymphocytes: how they develop and function.* Blood, 2008. **112**(5): p. 1570-80.
4. Bonilla, F.A. and H.C. Oettgen, *Adaptive immunity.* Journal of Allergy and Clinical Immunology, 2010. **125**(2, Supplement 2): p. S33-S40.
5. Pieper, K., B. Grimbacher, and H. Eibel, *B-cell biology and development.* Journal of Allergy and Clinical Immunology, 2013. **131**(4): p. 959-971.
6. Holmes, M.L., C. Pridans, and S.L. Nutt, *The regulation of the B-cell gene expression programme by Pax5.* Immunol Cell Biol, 2008. **86**(1): p. 47-53.
7. Sandel, P.C. and J.G. Monroe, *Negative selection of immature B cells by receptor editing or deletion is determined by site of antigen encounter.* Immunity, 1999. **10**(3): p. 289-99.
8. Methot, S.P. and J.M. Di Noia, *Molecular Mechanisms of Somatic Hypermutation and Class Switch Recombination.* Adv Immunol, 2017. **133**: p. 37-87.
9. Fozza, C., et al., *Study of the T-cell receptor repertoire by CDR3 spectratyping.* Journal of Immunological Methods, 2017. **440**: p. 1-11.
10. Gerondakis, S., et al., *NF-kappaB control of T cell development.* Nat Immunol, 2014. **15**(1): p. 15-25.
11. Qiu, H., et al., *Transcriptional and epigenetic regulation of follicular T-helper cells and their role in autoimmunity.* Autoimmunity, 2017. **50**(2): p. 71-81.
12. Andersen, M.H., et al., *Cytotoxic T cells.* J Invest Dermatol, 2006. **126**(1): p. 32-41.
13. Schatz, D.G. and Y. Ji, *Recombination centres and the orchestration of V(D)J recombination.* Nat Rev Immunol, 2011. **11**(4): p. 251-63.
14. Roth, D.B., *V(D)J Recombination: Mechanism, Errors, and Fidelity.* Microbiol Spectr, 2014. **2**(6).
15. Arya, R. and C.H. Bassing, *V(D)J Recombination Exploits DNA Damage Responses to Promote Immunity.* Trends Genet, 2017. **33**(7): p. 479-489.
16. Malu, S., et al., *Role of non-homologous end joining in V(D)J recombination.* Immunologic Research, 2012. **54**(1): p. 233-246.
17. Lindahl, T., *Instability and decay of the primary structure of DNA.* Nature, 1993. **362**(6422): p. 709-15.
18. Iyama, T. and D.M. Wilson, 3rd, *DNA repair mechanisms in dividing and non-dividing cells.* DNA Repair (Amst), 2013. **12**(8): p. 620-36.
19. Rulten, S.L. and G.J. Grundy, *Non-homologous end joining: Common interaction sites and exchange of multiple factors in the DNA repair process.* Bioessays, 2017. **39**(3).
20. Bohgaki, T., M. Bohgaki, and R. Hakem, *DNA double-strand break signaling and human disorders.* Genome Integr, 2010. **1**(1): p. 15.
21. Cannan, W.J. and D.S. Pederson, *Mechanisms and Consequences of Double-Strand DNA Break Formation in Chromatin.* J Cell Physiol, 2016. **231**(1): p. 3-14.
22. Filippo, J.S., P. Sung, and H. Klein, *Mechanism of Eukaryotic Homologous Recombination.* Annual Review of Biochemistry, 2008. **77**(1): p. 229-257.
23. Kumar, V., F.W. Alt, and V. Oksenych, *Reprint of "Functional overlaps between XLF and the ATM-dependent DNA double strand break response".* DNA Repair (Amst), 2014. **17**: p. 52-63.
24. Oksenych, V., et al., *Functional redundancy between the XLF and DNA-PKcs DNA repair factors in V(D)J recombination and nonhomologous DNA end joining.* Proc Natl Acad Sci U S A, 2013. **110**(6): p. 2234-9.

25.   Pannunzio, N.R., G. Watanabe, and M.R. Lieber, *Nonhomologous DNA end-joining for repair of DNA double-strand breaks.* J Biol Chem, 2018. **293**(27): p. 10512-10523.

26.   Ochi, T., et al., *DNA repair. PAXX, a paralog of XRCC4 and XLF, interacts with Ku to promote DNA double-strand break repair.* Science, 2015. **347**(6218): p. 185-188.

27.   Gago-Fuentes, R., et al., *Normal development of mice lacking PAXX, the paralogue of XRCC4 and XLF.* FEBS Open Bio, 2018. **8**(3): p. 426-434.

28.   Aceytuno, R.D., et al., *Structural and functional characterization of the PNKP-XRCC4-LigIV DNA repair complex.* Nucleic Acids Res, 2017. **45**(10): p. 6238-6251.

29.   Agarwal, S., et al., *Isolation, characterization, and genetic complementation of a cellular mutant resistant to retroviral infection.* Proceedings of the National Academy of Sciences, 2006. **103**(43): p. 15933-15938.

30.   Slavoff, S.A., et al., *A human short open reading frame (sORF)-encoded polypeptide that stimulates DNA end joining.* J Biol Chem, 2014. **289**(16): p. 10950-7.

31.   Grundy, G.J., et al., *The Ku-binding motif is a conserved module for recruitment and stimulation of non-homologous end-joining proteins.* Nat Commun, 2016. **7**: p. 11242.

32.   Arnoult, N., et al., *Regulation of DNA repair pathway choice in S and G2 phases by the NHEJ inhibitor CYREN.* Nature, 2017. **549**(7673): p. 548-552.

33.   Hung, P.J., et al., *MRI Is a DNA Damage Response Adaptor during Classical Non-homologous End Joining.* Molecular cell, 2018. **71**(2): p. 332-342. e8.

34.   Abramowski, V., et al., *PAXX and Xlf interplay revealed by impaired CNS development and immunodeficiency of double KO mice.* Cell Death Differ, 2018. **25**(2): p. 444-452.

35.   Frank, K.M., et al., *DNA ligase IV deficiency in mice leads to defective neurogenesis and embryonic lethality via the p53 pathway.* Mol Cell, 2000. **5**(6): p. 993-1002.

36.   Carvalho, S., et al., *SETD2 is required for DNA double-strand break repair and activation of the p53-mediated checkpoint.* Elife, 2014. **3**: p. e02482.

37.   Menon, V. and L. Povirk, *Involvement of p53 in the repair of DNA double strand breaks: multifaceted Roles of p53 in homologous recombination repair (HRR) and non-homologous end joining (NHEJ).* Subcell Biochem, 2014. **85**: p. 321-36.

38.   Gao, Y., et al., *Interplay of p53 and DNA-repair protein XRCC4 in tumorigenesis, genomic stability and development.* Nature, 2000. **404**(6780): p. 897-900.

39.   Castaneda-Zegarra, S., et al., *Synthetic lethality between DNA repair factors Xlf and Paxx is rescued by inactivation of Trp53.* DNA Repair (Amst), 2019. **73**: p. 164-169.

40.   Xing, M., et al., *Synthetic lethality between murine DNA repair factors XLF and DNA-PKcs is rescued by inactivation of Ku70.* DNA Repair, 2017. **57**: p. 133-138.

41.   Sugo, N., et al., *p53 Deficiency Rescues Neuronal Apoptosis but Not Differentiation in DNA Polymerase β-Deficient Mice.* Molecular and Cellular Biology, 2004. **24**(21): p. 9470-9477.

42.   Cipe, F.E., et al., *Cernunnos/XLF Deficiency: A Syndromic Primary Immunodeficiency.* Case Rep Pediatr, 2014. **2014**: p. 614238.

43.   O'Driscoll, M., et al., *DNA ligase IV mutations identified in patients exhibiting developmental delay and immunodeficiency.* Mol Cell, 2001. **8**(6): p. 1175-85.

44.   Riballo, E., et al., *Cellular and biochemical impact of a mutation in DNA ligase IV conferring clinical radiosensitivity.* J Biol Chem, 2001. **276**(33): p. 31124-32.

45.   Saito, S., A. Kurosawa, and N. Adachi, *Mutations in XRCC4 cause primordial dwarfism without causing immunodeficiency.* Journal of human genetics, 2016. **61**(8): p. 679.

46.   Moshous, D., et al., *Artemis, a novel DNA double-strand break repair/V (D) J recombination protein, is mutated in human severe combined immune deficiency.* Cell, 2001. **105**(2): p. 177-186.

47.   Buck, D., et al., *Cernunnos, a novel nonhomologous end-joining factor, is mutated in human immunodeficiency with microcephaly.* Cell, 2006. **124**(2): p. 287-299.

48.   van der Burg, M., et al., *A DNA-PKcs mutation in a radiosensitive T–B–SCID patient inhibits Artemis activation and nonhomologous end-joining.* The Journal of clinical investigation, 2009. **119**(1): p. 91-98.

49. Woodbine, L., et al., *PRKDC mutations in a SCID patient with profound neurological abnormalities.* The Journal of clinical investigation, 2013. **123**(7): p. 2969-2980.

50. Eriksson, P.S., et al., *Neurogenesis in the adult human hippocampus.* Nat Med, 1998. **4**(11): p. 1313-7.

51. Doetsch, F., J.M. Garcia-Verdugo, and A. Alvarez-Buylla, *Cellular composition and three-dimensional organization of the subventricular germinal zone in the adult mammalian brain.* J Neurosci, 1997. **17**(13): p. 5046-61.

52. Alvarez-Buylla, A. and D.A. Lim, *For the long run: maintaining germinal niches in the adult brain.* Neuron, 2004. **41**(5): p. 683-6.

53. Morshead, C.M., C.G. Craig, and D. van der Kooy, *In vivo clonal analyses reveal the properties of endogenous neural stem cell proliferation in the adult mammalian forebrain.* Development, 1998. **125**(12): p. 2251-61.

54. Kaneko, N. and K. Sawamoto, *Adult neurogenesis and its alteration under pathological conditions.* Neuroscience Research, 2009. **63**(3): p. 155-164.

55. Homem, C.C.F., M. Repic, and J.A. Knoblich, *Proliferation control in neural stem and progenitor cells.* Nature Reviews Neuroscience, 2015. **16**: p. 647.

56. Sun, D., et al., *Regulation of neural stem cell proliferation and differentiation by Kinesin family member 2a.* PLoS One, 2017. **12**(6): p. e0179047.

57. He, S., D. Nakada, and S.J. Morrison, *Mechanisms of stem cell self-renewal.* Annu Rev Cell Dev Biol, 2009. **25**: p. 377-406.

58. Morrison, S.J. and J. Kimble, *Asymmetric and symmetric stem-cell divisions in development and cancer.* Nature, 2006. **441**(7097): p. 1068-1074.

59. Wen, S., H. Li, and J. Liu, *Dynamic signaling for neural stem cell fate determination.* Cell Adh Migr, 2009. **3**(1): p. 107-17.

60. Wang, W., et al., *Mitochondrial DNA Damage Level Determines Neural Stem Cell Differentiation Fate.* The Journal of Neuroscience, 2011. **31**(26): p. 9746-9751.

61. Li, G., et al., *Lymphocyte-specific compensation for XLF/cernunnos end-joining functions in V (D) J recombination.* Molecular cell, 2008. **31**(5): p. 631-640.

62. Gao, Y., et al., *A targeted DNA-PKcs-null mutation reveals DNA-PK-independent functions for KU in V (D) J recombination.* Immunity, 1998. **9**(3): p. 367-376.

63. Gago-Fuentes, R., et al., *Normal development of mice lacking PAXX, the paralogue of XRCC 4 and XLF.* FEBS Open Bio, 2018. **8**(3): p. 426-434.

64. Jacks, T., et al., *Tumor spectrum analysis in p53-mutant mice.* Current biology, 1994. **4**(1): p. 1-7.

65. Wang, W., et al., *Mitochondrial DNA Integrity Is Essential For Mitochondrial Maturation During Differentiation of Neural Stem Cells.* STEM CELLS, 2010. **28**(12): p. 2195-2204.

66. Gao, Y., et al., *A critical role for DNA end-joining proteins in both lymphogenesis and neurogenesis.* Cell, 1998. **95**(7): p. 891-902.

67. Golmohammadi, M.G., et al., *Comparative analysis of the frequency and distribution of stem and progenitor cells in the adult mouse brain.* Stem Cells, 2008. **26**(4): p. 979-87.

68. Carreira, B.P., et al., *Nitric oxide stimulates the proliferation of neural stem cells bypassing the epidermal growth factor receptor.* Stem Cells, 2010. **28**(7): p. 1219-30.

69. Reynolds, B.A. and R.L. Rietze, *Neural stem cells and neurospheres--re-evaluating the relationship.* Nat Methods, 2005. **2**(5): p. 333-6.

70. Irvin, D.K., et al., *Extrinsic and intrinsic factors governing cell fate in cortical progenitor cultures.* Dev Neurosci, 2003. **25**(2-4): p. 162-72.

71. Morshead, C.M., et al., *Hematopoietic competence is a rare property of neural stem cells that may depend on genetic and epigenetic alterations.* Nat Med, 2002. **8**(3): p. 268-73.

72. Vukicevic, V., et al., *Genetic instability and diminished differentiation capacity in long-term cultured mouse neurosphere cells.* Mech Ageing Dev, 2010. **131**(2): p. 124-32.

73. Fields, R.D. and M.V. Lancaster, *Dual-attribute continuous monitoring of cell proliferation/cytotoxicity.* Am Biotechnol Lab, 1993. **11**(4): p. 48-50.

74.   Chen, H., et al., *Ionizing Radiation Perturbs Cell Cycle Progression of Neural Precursors in the Subventricular Zone Without Affecting Their Long-Term Self-Renewal.* ASN Neuro, 2015. **7**(3).

75.   Palmer, T.D., et al., *Cell culture. Progenitor cells from human brain after death.* Nature, 2001. **411**(6833): p. 42-3.

76.   Sanai, N., et al., *Unique astrocyte ribbon in adult human brain contains neural stem cells but lacks chain migration.* Nature, 2004. **427**(6976): p. 740-4.

77.   Suslov, O.N., et al., *Neural stem cell heterogeneity demonstrated by molecular phenotyping of clonal neurospheres.* Proc Natl Acad Sci U S A, 2002. **99**(22): p. 14506-11.

78.   Ming, G.L. and H. Song, *Adult neurogenesis in the mammalian brain: significant answers and significant questions.* Neuron, 2011. **70**(4): p. 687-702.

Appendixes

Appendix A:

Primer sequences and expected WT and mutant amplifications of *Paxx*, *Xlf*, *Dna-pkcs* and *Trp53*.

Primers	Sequence	Amplicons
Paxx Forward	ACAGAGGGTGGTGACTCAGACAATGG	WT 965bp / Mutant 329, 312, or 295bp
Paxx Reverse	ACAGAGGGTGGTGACTCAGACAATGG	
Xlf WT	CATGTTGGCTCTGCGAATAGA	WT 650bp / Mutant 950bp
Xlf Mutant	CTGTCTTGTGGGCATAGTAGGC	
Xlf Common	GAGCTCGGATATGAGCGCTCAG	
Dna-pkcs WT	GAAAAAGTCTATGAGCTCCTGGGAG	WT 250bp / Mutant 427bp
Dna-pkcs Mutant	ACGTAACTCCTCTTCAGACCT	
Dna-pkcs Common	CCCTCCAGACAGCCAGCTAAGACAGG	
Trp53 WT	AGGCTTAGAGGTGCAAGCTG	WT 321bp / Mutant 150bp
Trp53 Mutant	CAGCCTCTGTTCCACATACACT	
Trp53 Common	TGGATGGTGGTATACTCAGAGC	

Appendix B:
PCR Programs.

A.

Paxx (WT/Mutant)			
Step	**Time**	**Temperature (°C)**	**Cycles**
Initial denaturation	2 min	94	1
Denaturation	30 sec	94	30
Annealing	45 sec	68	
Elongation	1 min	72	
Final extension	5 min	72	1
Hold	∞	4	

B.

Xlf (WT/Mutant)			
Step	**Time**	**Temperature (°C)**	**Cycles**
Initial denaturation	3 min	95	1
Denaturation	30 sec	95	40
Annealing and elongation	1 min	62	
Final extension	5 min	68	1
Hold	∞	4	

C.

Dna-pkcs WT			
Step	**Time**	**Temperature (°C)**	**Cycles**
Initial denaturation	3 min	94	1
Denaturation	45 sec	94	30
Annealing	45 sec	66	
Elongation	1 min	72	
Final extension	5 min	72	1
Hold	∞	4	

D.

Dna-pkcs Mutant			
Step	**Time**	**Temperature (ºC)**	**Cycles**
Initial denaturation	3 min	94	1
Denaturation	45 sec	94	
Annealing	45 sec	59,6	40
Elongation	1 min	72	
Final extension	5 min	72	1
Hold	∞	4	

E.

Trp53 (WT/Mutant)			
Step	**Time**	**Temperature (ºC)**	**Cycles**
Initial denaturation	2 min	95	1
Denaturation	30 sec	95	
Annealing	30 sec	67	30
Elongation	20 sec	72	
Final extension	5 min	72	1
Hold	∞	4	